The Mechanism of Hydrogen Embrittlement in Steel

By

A. S. Tetelman+

Department of Materials Science

Stanford University

Stanford, California

July, 1967

Technical Report #7

Prepared for the National Aeronautics and Space Agency

Under NASA Grant NSG-622

ABSTRACT

The process of brittle fracture in structural materials can be separated into three stages; 1) crack nucleation, 2) slow crack growth, and 3) rapid, unstable fracture. Hydrogen embrittles steel by affecting the first two of these stages. In corroded, electrolytically charged, or thermally charged specimens, excess hydrogen precipitates at inclusions or carbides in molecular form, causing the initiation of voids or microcracks. The hydrogen pressure in these defects causes them to grow either by plastic deformation or by cleavage, depending on the intrinsic toughness of the particular steel and the shape of the nucleating particle. It is shown that the size of the defects is determined by the spacing of the nucleating particles. Consequently, small voids or cracks will exist when a given volume of second phase is finely distributed. In hot rolled materials, alignment of inclusions can be used to minimize hydrogen embrittlement.

Microcrack or void coalescence, to form a macrocrack, occurs when a stress is applied to a hydrogenated structure. The effect of hydrogen concentration, applied stress, notch geometry, strength level, temperature, and microstructure on the incubation time for slow crack growth, the rate of slow crack growth, and the time to fail in a static test or the tensile ductility are considered. Finally, crack growth in external environments, such as hydrogen gas, is also discussed briefly.

I. INTRODUCTION

During the corrosion process electrons are freed at anodic sites on the metal surface, flow through the metal, and cause a reduction of charged ions at cathodic sites on the surface. While the oxidation processes that occur at the local anode are of great importance in the stress corrosion cracking process, the cathodic reactions are of little importance, provided that the cathode does not become polarized. However, when high strength ferritic or martensitic steels corrode in strongly acidic (pH<4) or strongly alkaline (pH>10) solutions, hydrogen ions are reduced to hydrogen atoms at the local cathode. These atoms are able to diffuse into the metal and, in the presence of a sufficiently high stress, cause cracking and even total failure of the structure. This phenomena is known as hydrogen embrittlement. Some of the most spectacular instances of hydrogen embrittlement have occurred in oil well casing and tubing, particularly in natural gas wells that contain H_2S.[1]

In addition to the hydrogen embrittlement that can accompany stress corrosion cracking, numerous failures of cadmium plated high strength steel parts, where the hydrogen was introduced during electroplating, have also been reported.[2-5] Hydrogen cracking has also been observed in cast structures when a substantial amount of hydrogen was retained during solidification, particularly in massive castings[6] and in rapidly cooled weld metal.[7-9] More recently, two additional types of hydrogen embrittlement have been noted. First, there is the embrittlement of high strength steel in the presence of water vapor[10-14] or pure hydrogen at one atmosphere pressure. Secondly, there is the

embrittlement that occurs in the presence of high pressure hydrogen gas.[15-19]

Since hydrogen embrittlement is one of the most serious forms of time-dependent fracture, a considerable effort has been made to understand the mechanism of cracking. Most of the interpretable research has been performed on plain or notched tensile specimens that were electrolytically (cathodically) charged with hydrogen and consequently the major portion of this review will be concerned with cathodically charged specimens.

In laboratory testing, the embrittlement appears as a decreased tensile ductility (reduction in area) in a tensile test (Figure 1), a decrease in notch tensile strength, and as a delayed failure in a static loading test (Figure 2). The yield strength is relatively unaffected by the presence of hydrogen. As shown in Figure 1, the effect of hydrogen becomes more severe as the strength level of the steel increases.

Several theories have been proposed to explain the mechanism of embrittlement. These theories, as well as most of the significant experimental work, have been reviewed in several extensive treatments during the past decade.[20-26] Basically, the theories fall into two groups. First, there is the "pressure theory" originally proposed by Zapffe,[27] subsequently modified by de Kazinsky,[28] Garofalo et al,[29] Bilby and Hewitt,[30] and Tetelman and Robertson.[31,32] This theory proposes that hydrogen embrittlement results from the precipitation of hydrogen gas at defects such as inclusions, and the expansion of microcracks and voids due to the gas pressure. In this model, the internal pressure, P, lowers the applied stress, σ_F, necessary to cause crack

growth. Thus, below the yield strength σ_Y, unstable fracture occurs from the tip of a stopped crack[26] when

$$\sigma_F + P = \sqrt{\frac{2 E \gamma_p^*}{\pi c}} \qquad (\sigma \ll \sigma_Y) \tag{1}$$

where 2c is the crack length, E is the elastic modulus and γ_p^* is the work done in initiating unstable fracture at the crack tip. Alternatively, when hydrogen is present inside a microcrack formed by dislocation pile-ups, the pressure P reduces the stress σ_G required for microcrack growth[26,29,30]

$$\sigma_G = \frac{2 \gamma_m}{n b} - P \tag{2}$$

where n is the number of dislocations in the pile up having Burgers' vector b and γ_m is the work done in microcrack propagation. γ_m is directly proportional to the true surface energy, γ_s.

Secondly, there is the "decreasing strength theory" of Petch and Staples,[33] Bastien[20] and Troiano.[21] This theory proposes that the presence of dissolved hydrogen lowers the cohesive strength of the iron lattice, in a manner similar to that which occurs in liquid metal embrittlement. In this model, the decrease in cohesive strength results in a decrease in the surface energy of fracture and hence in a lowering of the applied stress necessary for crack propagation. Thus for pre-existing cracks

$$\sigma_F = \sqrt{\frac{2 E \gamma_p^*(H)}{\pi c}} \qquad (\sigma \ll \sigma_Y) \tag{3}$$

and for microcracks formed by plastic deformation

$$\sigma_G \, n \, b = 2 \gamma_m(H) \tag{4}$$

where $\gamma_p^*(H)$ and $\gamma_m(H)$ signify a lowering of the work expended in crack propagation and microcrack growth in the presence of hydrogen.

Since both models predict a lowering in the stress necessary for crack propagation it is very difficult to separate them experimentally. It is well known, however, that microcracks can be formed in the absence of applied stress, simply by the presence of hydrogen concentrations in excess of the solubility limit[23,24,26-32] (Figure 3). It is difficult to see how these cracks could have been formed if there were no gas expansion to provide the work required to open the crack. Thus, while it is possible that dissolved hydrogen can affect the strength of atomic bonds, there is no evidence that it does so and some evidence from X-ray[34] and diffusion[35], low temperature fracture[36], and surface conductance[71] studies that it does not.

Troiano and his co-workers[21,37-39] have presented several valid objections to the original pressure theory; principally, that hydrogen induced crack growth occurs slowly and discontinuously and that the diffusion of hydrogen to regions of tri-axial stress in front of a growing crack is a significant factor in the embrittlement process. The original pressure theory, based on the rapid propagation of a crack when equation (1) is satisfied, or the formation of an unstable microcrack when equation (2) is satisfied, cannot account for these objections. However, a modified form of the pressure theory need not be inconsistent with the fact that hydrogen induced crack propagation occurs slowly and discontinuously, as will be shown below. In section II some of the mechanisms of crack propagation in metals are discussed. The significant experimental observations of hydrogen embrittlement in charged specimens

are then reviewed in sections III and IV and these observations are used to develop a self consistent mechanism for hydrogen embrittlement. Finally in section V, some discussion of hydrogen embrittlement in an external environment (e.g., stress corrosion cracking) is presented.

II. THE MECHANICS OF CRACK PROPAGATION AND FRACTURE

The process of brittle fracture in structural materials can be separated into three stages; crack nucleation, slow crack growth, and rapid, unstable fracture.

A. Crack Nucleation

In flaw free materials, the first stage in the fracture process is the nucleation of a microcleavage crack or void. These defects are formed by the piling up and coalescence of dislocation groups in the vicinity of grain boundaries or hard particles such as inclusions.[25,40] As the applied stress (in a tensile test) or strain increases, increasing numbers of microcracks and voids are formed.[41,42,43] These act as strain concentrators which cause the material between them to fail in shear at low nominal strains (Figure 4).[44] Eventually, a sufficient number of voids and/or microcracks have formed and coalesced to lead to the development of a macrocrack (crack) about five grain diameters in length.

B. Slow Crack Growth

Crack growth initially occurs discontinuously.[44] Increasing numbers of voids form ahead of its tip and join to it (coalesce). Crack propagation occurs by short, rapid advances (coalescence) followed by waiting periods in which the plastic strain ahead of the crack builds up sufficiently to cause void formation and local instability.[26,44]

C. Rapid Fracture

As the crack grows longer, its ability to concentrate strain at its tip increases. Eventually, the crack is long enough to satisfy the criteria for unstable fracture (see below) and propagate rapidly, causing the structure to fail. The critical crack length at which this occurs is labeled ($2c_F$) in subsequent discussion.

There are certain cases under which only one or two of these processes is observed. For example, at temperatures well below the ductile-brittle transition in BCC metals, the first microcrack that forms is able to spread unstably both through the grain in which it was nucleated and the boundary surrounding this grain, causing an unstable fracture without any detectable slow crack growth.[40,42] Stage B is then not detected (Figure 5a). The criterion for this to occur is then the same as the criterion for the initial growth of microcrack; namely that the applied tensile stress reach a value σ_G, given by equation (2) with $P = 0$.

Most structural materials contain flaws that have been introduced by machining, improper welding, fabrication defects, etc. In this case, stage A is absent and fracture involves the slow growth of the flaw of length $c = c_o$ at a stress $\sigma = \sigma_1$ until $c = c_F$ and rapid fracture can occur. This process of discontinuous, slow crack growth occurs under increasing stress (Figure 5b) in a tensile test or over a period of increasing time in a static test (Figure 5c).

The microscopic aspects of crack propagation depend on the type of material, the test temperature, and the yield strength level of the material. In BCC metals such as steel, fracture at low temperatures

involves the nucleation and fast propagation, or nucleation, coalescence and fast propagation of microcleavage cracks. As the temperature increases, the yield strength σ_Y decreases. Since the stress level ahead of an advancing crack σ_{yy} can be no higher than about 2.5 σ_Y, assuming full triaxiality, the stress level at the crack tip decreases with increasing temperature. At some critical temperature the stresses are too low to cause microcleavage crack formation, and fracture occurs by the formation of voids at inclusions and the coalescence of these voids by plastic strain concentration.[26,40,45] Since void formation and coalescence involve larger local strains and hence absorb more energy than cleavage, the toughness or impact energy increases with increasing temperature (Figure 6). In low yield strength materials ($\sigma_Y < \frac{E}{300}$) the process of void formation and coalescence absorbs so much energy that the transition from cleavage to shear is a brittle-ductile transition. However, in high strength materials ($\sigma_Y > \frac{E}{300}$) the tensile stress level in the plastic zone ahead of the advancing crack is so high that a high density of voids form at temperatures where cleavage cannot occur. Consequently, smaller strains are involved in void coalescence (Figure 7) and the toughness is low. In this case, the cleavage to shear transition is <u>not</u> brittle-ductile transition (Figure 6).

The principles of <u>fracture mechanics</u> have been used to determine the macroscopic criteria for the unstable propagation of a crack (stage C). It has been shown[46,51] that unstable fracture occurs when the crack opening displacement at the crack tip, 2V(c), reaches a critical value, 2V*(c). Thus the fracture criterion becomes

$$V(c) = V^*(c) \qquad (5)$$

Since the tensile stress level in the plastic zone is of the order of the yield strength, the amount of work done at the crack tip is

$$G \cong 2\sigma_Y V(c)$$

and consequently the critical amount of work done in unstable fracture is

$$G_c \cong 2 \sigma_Y V^*(c) \tag{7}$$

The methods of linear elastic fracture mechanics[50,52] indicate that unstable fracture can occur before general yield ($\sigma_F < \sigma_Y$) when

$$K^2 = E G_c = K_c^2 \tag{8}$$

where K is known as the stress intensity factor

$$K = \sigma\sqrt{\alpha \pi c} \tag{9}$$

and K_c, the critical value of K at which instability occurs, is known as the fracture toughness:

$$K_c = \sigma_F \sqrt{\alpha \pi c_F} \tag{10}$$

α is an orientation factor that accounts for notch and structure geometry.[26,53] At low stress levels ($\sigma_F \ll \sigma_Y$) $\alpha \cong 1$ so that

$$\sigma_F = \sqrt{\frac{EG_c}{\pi c}} \qquad (\sigma_F \ll \sigma_Y) \tag{11}$$

Note that this is the same form as equation (1) with $G_c = 2\gamma_p^*$ and P = 0. Introducing (7) gives

$$\sigma_F = \sqrt{\frac{2 E \sigma_Y V^*(c)}{\pi c}} \qquad (\sigma_F < \sigma_Y) \tag{12}$$

It is apparent from equation (12) that once the critical displacement 2V*(c) has been achieved, the crack will spread rapidly at $\sigma = \sigma_F$, since an increase in c decreases the stress required for propagation and the

process is instable.

At the present time there are no general analytic expressions that can be used to describe fracture behavior after general yielding has occurred (i.e., when $\sigma_F > \sigma_Y$). Assuming that a critical displacement criteria is applicable, one can treat the crack as a strain concentrator so that the ductility ϵ_F is that nominal strain which is required to produce the critical displacement $2V^*(c)$ at the crack tip; σ_F is then the nominal stress required to achieve a given ϵ_F, due to strain hardening.[26]

The physical meaning of a critical displacement criterion for unstable fracture has been the subject of much discussion.[46-51] A simple interpretation[47,48] is that the volume element of material at the crack tip behaves as a minature tensile specimen whose gauge length, under local plane strain deformation, is of the order of twice the tip radius ρ of the advancing crack. Consequently, a crack tip strain $\epsilon(c)$ produces a crack opening displacement

$$2V(c) = 2\,\rho\,\epsilon(c). \tag{13}$$

Unstable fracture occurs when the crack tip strain builds up to a critical value $\epsilon_f(c)$[44] which is proportional to, but not necessarily equal to, the ductility of a plane tensile specimen ϵ_f, measured under identical conditions. Consequently, from equation (5)

$$V^*(c) = \rho\,\epsilon_f(c) \tag{14}$$

and thus the plane strain toughness G_{Ic} is

$$G_{Ic} \cong 2\,\sigma_Y\,\rho\,\epsilon_f(c). \tag{15}$$

Under certain conditions, particularly in the presence of reactive environments or under alternating loading (fatigue), stable (slow)

crack propagation can occur when the crack tip strain is less than $\epsilon_f(c)$ and the crack tip displacement is less than $V^*(c)$.[26,44] As the crack grows, its stress intensity factor K and hence its tip displacement V(c) increase. Eventually, V(c) equals $V^*(c)$ and the propagation becomes unstable; this marks the transition from stage B to stage C described above.

Suppose that a crack of length $2c_o$ exists in a structure subjected to a tensile stress σ that is less than σ_Y. If the rate of slow crack growth $(^{dc}/dt)$ is known, then the time t_F at which the structure will fail is determined by the condition that $c = c_F$ at $t = t_F$. For example, when $(^{dc}/dt) = A$ is a constant, failure will occur when

$$c_o + A\, t_F = c_F = \frac{EG_c}{\alpha \pi \sigma^2} \tag{16}$$

and hence

$$t_F = \left[\frac{EG_c}{\alpha \pi \sigma^2} - c_o\right] \frac{1}{A} \tag{17}$$

Thus, a decrease in fracture toughness or an increase in applied stress leads to a decrease in lifetime, even if the rate of slow crack growth is unchanged.

In certain instances, particularly in the stress corrosion cracking of alpha brass in ammonium sulfate[54] or the embrittlement of high strength steel in the presence of water vapor[12], the rate of slow crack growth increases with stress intensity factor (Figure 8) and hence as the crack length increases under a constant applied stress. For those cases where $(^{dc}/dt)$ is linearly proportional to K (Figure 8), we have

$$\frac{dc}{dt} = A' K \cong A \sigma' \sqrt{\alpha \pi c} \tag{18}$$

and hence

$$\int_{c_o}^{c_F} \frac{dc}{c^{\frac{1}{2}}} = A\sigma' \sqrt{\alpha \pi} \int_{o}^{t_F} dt \tag{19}$$

$$\tfrac{1}{2} (c_F^{\frac{1}{2}} - c_o^{\frac{1}{2}}) = A\sigma' \sqrt{\alpha \pi}\, t_F \tag{20}$$

so that

$$t_F = \frac{1}{2A'\sqrt{\alpha \pi}\,\sigma} \left[\left\{ \frac{EG_c}{\alpha \pi \sigma^2} \right\}^{\frac{1}{2}} - c_o^{\frac{1}{2}} \right] \tag{21}$$

Consequently, an increase in applied stress σ or growth constant A' and/or a decrease in fracture toughness G_c produces a decrease in the lifetime of the structure. The parameter A' can be strongly dependent upon environment (Figure 8). Finally, for those cases such as fatigue[54] where the rate of crack propagation is proportional to the square of the stress intensity factor

$$\frac{dc}{dt} = A'' K^2 = A'' \sigma^2 \alpha \pi c \tag{22}$$

$$\int_{c_o}^{c_F} \frac{dc}{c} = A'' \sigma^2 \alpha \pi \int_{o}^{t_F} dt \tag{23}$$

$$\ell n \left(\frac{c_F}{c_o} \right) = A'' \sigma^2 \alpha \pi\, t_F \tag{24}$$

$$t_F = \frac{1}{A'' \sigma^2 \alpha \pi} \ell n \left(\frac{EG_c}{\alpha \pi \sigma^2 c_o} \right) \tag{25}$$

and again t_F decreases with increasing A'' and σ and/or decreasing G_c.

The preceding analyses have shown how the lifetime may be determined when a flaw of length $2c_o$ is present at the time t = 0 that a stress σ is applied. In certain cases, particularly when hydrogen is introduced into a structure, the flaws do not exist initially but form after an incubation time, t_i.[21] If $2c_o$ is the flaw length at $t = t_i$, then equations (17, (21), and (25) must be modified to read:

$$t_F = \left[\frac{EG_c}{\alpha \pi \sigma^2} - c_o\right] \frac{1}{A} + t_i \qquad (26)$$

$$\left(\frac{dc}{dt} = A\right)$$

$$t_F = \frac{1}{2A' \sqrt{\alpha \pi \sigma}} \left[\left\{\frac{EG_c}{\alpha \pi \sigma^2}\right\}^{\frac{1}{2}} - c_o^{\frac{1}{2}}\right] + t_i \qquad (27)$$

$$\left(\frac{dc}{dt} = A'K\right)$$

$$t_F = \frac{1}{A'' \sigma^2 \alpha \pi} \ln \left(\frac{EG_c}{\alpha \pi \sigma^2 c_o}\right) + t_i \,. \qquad (28)$$

$$\left(\frac{dc}{dt} = A'' K^2\right)$$

Having developed equations which can predict the lifetime of a structure in terms of measurable parameters such as t_i, A, etc., it is possible to treat the problem of hydrogen embrittlement in terms of the effect of hydrogen on these parameters. In the following section we consider the problem of hydrogen induced crack nucleation, and the incubation time for crack formation under static loading (Stage A) in cathodically charged specimens. We then discuss the effect of hydrogen on the slow crack growth process (Stage B) and the conditions for final fracture. Finally, we consider the effect of an external hydrogen environment on the growth of cracks, as in the case of stress corrosion cracking.

III. THE MECHANISM OF HYDROGEN INDUCED CRACK FORMATION IN THE ABSENCE OF APPLIED STRESS

The equilibrium solubility C_H (in ppm) of hydrogen located in interstitial sites in the iron lattice varies with temperature T(°K) and external hydrogen pressure P_e (in atmospheres) as[55]

$$C_H = 42.7\, P_e^{\frac{1}{2}} \exp\left(-\frac{6500}{RT}\right) \qquad (29)$$

Above 150°C, the diffusivity D_H (cm^2 per sec) of hydrogen in iron also increases exponentially with temperature[35] according to the relation

$$D_H = 1.4 \times 10^{-3} \exp\left(-\frac{3200}{RT}\right) . \qquad (30)$$

$(T > 423°K)$

Measurements of the diffusivity by the gas effusion technique have shown that below 150°C the diffusivity decreases sharply, and varies with temperature as

$$D_H = 0.12 \exp\left(-\frac{7820}{RT}\right). \qquad (31)$$

$(T < 423°K)$

These observations suggest that the excess (above the solubility limit) hydrogen resides in "traps" and that below 150°C the diffusivity, as measured by gas effusion, is dependent upon the rate of release of hydrogen from these traps. Recent work[31,32] has shown that large voids or cracks are created by the expansion of hydrogen gas that has precipitated out of the iron lattice (Figure 3), and it is reasonable to associate these voids with the traps that cause the anamalous diffusion behavior.

Consider an iron specimen heated at a high temperature T_1 in the presence of 1 atmosphere of hydrogen gas (thermally charged) and then rapidly cooled (quenched) to room temperature T_2. Immediately after quenching the hydrogen content of the specimen $C_H(T_1) = C_H$ will be greater than the equilibrium content $C_H(T_2) = C_{eq}$ at $T = T_2$. Since there is no evidence for hydride formation in iron base alloys,[34] equilibrium can be achieved only when the excess hydrogen $(C_H - C_{eq})$ diffuses out of the iron lattice. Hydrogen atoms quenched into regions near to the specimen surface will be able to diffuse out to the surface,

recombine with other atoms to form molecular hydrogen, and escape into the atmosphere. However, excess hydrogen atoms in the interior of the specimen are closer to internal surfaces, such as the interfaces between inclusions (or carbides) and the lattice; they will diffuse to these surfaces, recombine with other hydrogen atoms to form H_2 gas, and precipitate inside the specimen as molecular hydrogen.

Similarly, during cathodic charging (e.g., an electroplating operation) or during certain corrosion reactions, hydrogen ions are reduced to hydrogen atoms at the metal surface. Most of these atoms recombine with others and are evolved as H_2 gas molecules. The remainder can be driven into the metal by the very high effective pressure (Fugacity) and precipitate internally in the form of voids or cracks. The total hydrogen content will be determined by the current density, the charging time and the surface condition, since the latter determines the rate of surface recombination to form the H_2 molecule and hence the driving force for H atoms to enter the steel. The presence of "poisons" such as sulfides and arsenic are particularly effective in preventing surface recombination and when present they increase the amount of absorbed hydrogen.

The presence of the hydrogen that has precipitated internally will be determined by the activity of the hydrogen atoms remaining in the lattice near the precipitation site, and by the constraints imposed by the mechanical properties of the material. Hydrogen atoms immediately adjacent to the inclusion precipitate out of the lattice until $C = C_{eq}$. This sets up a concentration gradient $[C_H - C_{eq}]$ which provides a driving force for diffusion to the interface. As increasing amounts of hydrogen

precipitate at the interface, the pressure P_H acting across the interface increases.

Although this local increase in pressure raises the equilibrium lattice concentration in the vicinity of the inclusion above C_{eq}, and the concentration of hydrogen away from the inclusion is decreased somewhat below C_H (Figure 9), there is still a large driving force for (1) subsequent diffusion of hydrogen to the interface, (2) further increases in the amount of H_2 gas that has precipitated and hence (3) further increases in the pressure set up across the interface.

Initially, the pressure produced in the interface region can be extremely high. For example, if a specimen at one atmosphere pressure is quenched from 1000°C to room temperature, C_H = 3.33 PPM, according to equation (29). The interface pressure that could exist in equilibrium with this lattice concentration at room temperature is 89,000 atm = 1.3×10^6 psi. Since this pressure is of the order of the theoretical cohesive strength, the interface between hard particles and the matrix will almost certainly be broken during the initial precipitation of the hydrogen, forming a void. Once the void has expanded (see below), the pressure inside it decreases and additional diffusion of hydrogen to the interface and precipitation of hydrogen gas at the void surface will occur. The number of moles that enter a circular void of radius r per unit time is

$$\frac{dn}{dt} = 4 \pi r_o^2 J \tag{32}$$

where at short times the flux J is given by[56]

$$J = D [C_H - C_{eq}] \left[\frac{1}{r_o} + \frac{1}{\sqrt{\pi Dt}} \right] . \tag{33}$$

For $r_o \cong 10^{-4}$ cm and $D = 5 \times 10^{-6}$ cm^2/sec (for untrapped hydrogen), $\frac{1}{r_o} \gg \frac{1}{\sqrt{\pi\ Dt}}$ at t = 1 sec so that

$$\frac{dn}{dt} \cong D[C_H - C_{eq}]\ 4\ \pi\ r_o. \tag{34}$$

Since the pressure inside the void is given by

$$P_H V = n\ RT \tag{35}$$

the rate of pressure build up is

$$\frac{dP_H}{dt} = \frac{RT}{V}\ \frac{dn}{dt} = \frac{3\ D}{r_o^{\,2}}\ RT\ [C_H - C_{eq}] \tag{36}$$

for spherical voids $V = \frac{4\ \pi\ r_o^{\,3}}{3}$, neglecting the volume of the inclusion when the radius of the voids is greater than about twice that of the inclusion. Taking C_H = 3.33 PPM and C_{eq} = 0.114 PPM (for a pressure of 50,000 psi inside the void, after the interface has broken and the void has expanded slightly), gives dP_H/dt = 500 atm./sec. for $r_o = 10^{-4}$cm, when R = 82.06 atm.cm^3/mole, °K and the hydrogen concentration is expressed in units of moles/cm^3 (1 PPM of hydrogen = 3.85×10^{-6} moles of H_2 that can precipitate out of a cubic centimenter of iron). This is very similar to the elastic loading rate that occurs in a conventional tensile test performed at an applied strain rate of 0.02 per min., i.e., 670 atm.per sec.

A. Void Expansion by Plastic Deformation

Under conditions where the iron lattice is inherently ductile and tough (e.g., pure iron at ambient temperature), the voids expand by plastic deformation and appear as speherical bubbles.[57] This condition is also favored if the precipitation site is spherical rather than pointed, since the stress concentration factor of the growing void will

then be too low to allow the void to transform into a brittle crack. The total pressure required for the growth of a void of radius r by plastic deformation is approximately[58]

$$P \cong \sigma_Y + \frac{2\gamma}{r} \tag{37}$$

where σ_Y is the yield strength and $(\frac{2\gamma}{r})$ is the force due to the surface tension of the void. Since $\gamma \cong 10^3$ ergs/cm^2, this term is negligibly small compared with σ_Y for voids larger than about 10^{-4}cm. Consequently, the void growth occurs when $P_H \approx \sigma_Y$, and consequently the number of moles of hydrogen required to produce a void of radius r is

$$n = \frac{\sigma_Y}{RT} \frac{4 \pi r^3}{3} , \tag{38}$$

again neglecting the volume of the inclusion inside the void. Suppose that hydrogen atoms enter the void from a spherical volume V* that surrounds it (Figure 10), and that (C_H V*) is the maximum number of moles that can enter the void.[+] V* is determined by the condition that beyond a distance r* for the particular void the hydrogen will diffuse to another void of the same size (Figure 10). Thus 2r* is approximately the inter void spacing and thus the maximum radius of the void, r_{max}, is determined by the condition

$$\frac{4}{3} \pi (r^*)^3 C_H = \frac{\sigma_Y}{RT} \frac{4}{3} \pi r^3_{max} \tag{39}$$

or

$$r_{max} = 1.2\ r^* \left(\frac{C_H}{\sigma_Y}\right)^{1/3} \tag{40}$$

for C_H in convenient units of PPM and σ_Y in units of psi, at room temperature. Thus for C_H = 3 PPM, σ_Y = 60,000 psi, r_{max} = 0.04, r* = 4 x 10^{-4} cm for an average void spacing r* of 10^{-2}cm. It should be pointed out that the voids will not form at <u>every</u> second-phase

particle (i) because of statisical considerations, and (ii) because once a void forms at a given particle, and the hydrogen pressure decreases, there will be a local driving force set up for diffusion to that particular void rather than to an adjacent one. Furthermore, the kinetics of hydrogen recombination and pressure build-up will vary from one void to another, because of variations in the structure of the interface. Thus we should expect that r* will be proportional to, but not equal to, the inter-particle spacing. Consequently, the maximum void size is limited by the spacing of the inclusions or other particles that serve as precipitation sites. When a given volume of second phase is finely distributed (r*small), the size of the voids will also be small. We should therefore expect that the degree of hydrogen embrittlement could be altered by variations in processing conditions, since the latter affect the size, shape and distribution of second phase particles. Similarly, the void size decreases as the amount of excess hydrogen decreases and as the yield strength increases.

B. Void Expansion by Brittle Crack Propagation

Many aspects of this problem have been discussed previously[23,31,32,59,60] and need not be repeated here. This type of expansion occurs in inherently brittle materials (such as monocrystalline iron-3% silicon at room temperature), and when the particles and inclusions that serve as precipitation sites are sharp rather than round. Brittle crack propagation usually begins in a discontinuous manner by the formation of a microcrack nucleus ahead of the advancing crack, due to dislocation pile-ups, and the coalescence of this crack nucleus with the advancing crack tip[59] (Figure 11). When the crack is sufficiently long and

sharp, large scale, rapid elastic propagation can occur. However, since essentially no hydrogen has time to enter the crack when it is moving, the pressure inside the crack decreases as the crack grows. Consequently, crack growth occurs until the pressure inside the crack drops below the Griffith value,equation (41); the crack then remains at rest until diffusion of hydrogen to it causes the pressure to build up sufficiently to re-start it, at which point elastic propagation can again take place. The pressure required for crack propagation is given by equation (1) with $\sigma = 0$.

$$P = \sqrt{\frac{2E\,\gamma^*_p}{\pi c}} \tag{41}$$

Since the volume of the crack V is

$$V \cong \frac{8\,P\,c^3}{3E} \tag{42}$$

the number of moles of hydrogen required to spread the crack is

$$n = \frac{8P^2c^3}{3E\,RT} = \frac{16}{3\pi}\,\frac{\gamma^*_p c^2}{RT} = 6.8 \times 10^{-11}\,\gamma^*_p c^2 \tag{43}$$

for γ^*_p in ergs/cm^2, T = 300°K and c in cm. Taking $\gamma^*_p = 10^4$ ergs/cm^2 as a typical value for the work required to propagate a sharp, stopped microcrack gives

$$n = 6.9 \times 10^{-7} c^2. \tag{44}$$

As in the case of void growth by plastic deformation, the maximum size to which the crack will grow can be estimated by assuming that the hydrogen enters the crack from a cylinder of length 2c and radius r*, where 2 r* is the spacing between parallel cracks. Thus

$$2c_{max}\,\pi(r^*)^2\,C_H = 6.9 \times 10^{-7} c^2$$

$$c_{max} = 35\,(r^*)\,2\,C_H \tag{45}$$

when C_H is again in convenient units of PPM. Thus, for C_H = 3 PPM, $r^* = 10^{-2}$cm, $c_{max} = 6 \times 10^{-3}$cm. As in the case of void growth by plastic flow, the growth of a brittle crack will be limited by the number of crack nuclei and the hydrogen concentration. Large scale crack propagation is possible in single crystals, where r* is large (say 1 cm), but in polycrystals, where r* is of the order of the grain size, c_{max} small.

The fact that hydrogen induced crack growth occurs along the interface between long, sharp inclusions and the matrix may have practical significance. In structures that are loaded uniaxially (e.g., drill pipe or casing), prior hot rolling will allign the inclusions parallel to the tensile axis. Any hydrogen cracks that form along these "fibers" will then be parallel to the tensile axis and coalescence by plastic strain concentration will be more difficult than if the cracks had lain perpendicular to the tensile axis.

IV. THE MECHANISM OF DELAYED FAILURE IN HYDROGENATED STEELS

A. The Incubation Time Required for the Start of Slow Crack Growth in the Presence of an Applied Stress

The preceding calculations have shown that in the absence of applied stress, excess hydrogen precipitates in small voids and cracks and causes these defects to grow out to a size that is dependent upon defect spacing and hydrogen concentration. We shall now examine the process of crack formation that occurs by the coalescence of these defects when a stress is applied to a hydrogenated material. It is most convenient to consider this process in terms of the delayed failure characteristics of notched tensile specimens of high strength steel. Troiano and his co-workers[21,37-39,61,62] have made electrical

resistance measurements as a function of time during static loading, and obtained curves such as those shown in Figure 12. Immediately after application of the stress, the electrical resistance increases, a phenomenon associated with the elastic and plastic deformation that occurs at the notch tip. Following this rise, the resistance remains constant for a certain period of time (the incubation time) after which it again increases incrementally as slow crack growth begins.

Although elastic and plastic deformation contribute to the increased resistance following the application of load, some of this increase is almost certainly associated with void coalescence, and hence in crack formation in regions of high triaxial stress beneath the notch root.[61] The formation of a crack by void coalescence causes the hydrogen pressure inside it to decrease below that which exists in voids that have not coalesced. This provides a driving force for diffusion of hydrogen from adjacent voids until the pressure in the crack has built up sufficiently to allow it to begin growing slowly. It has been shown[62] that the logarithm of the reciprocal of the incubation time t_i is proportional to the reciprocal of the absolute test temperature, indicating that the processes involved are thermally activated. The activation energy obtained from the data is 8900 cal/gm mole, consistent with the value for the diffusivity of trapped hydrogen at this temperature, 7800 cal/gm mole. Using the relation $x^2 = Dt$, it appears that hydrogen diffuses into the crack from a spherical volume whose radius is about 10^{-2} cm.

Figure 13 indicates that t_i is relatively independent of applied stress but strongly dependent upon hydrogen concentration, which was

varied by varying the degree of outgassing by baking after cathodic charging.[+] This is consistent with the fact that increasing hydrogen concentrations imply larger voids prior to application of stress (and perhaps more of them), and hence a larger crack after the application of stress. Consequently, a smaller amount of hydrogen needs to diffuse to the crack to cause it to grow slowly, in the presence of the high longitudinal stresses that exist beneath the notch root. In addition, a higher intial hydrogen concentration provides a higher flux of hydrogen to the crack and thereby shortens the amount of time required for the introduction of a given amount of hydrogen.

Figure 13 indicates that there is a lower limiting value of applied stress beneath which crack incubation does not occur. This stress level is the same as the lower critical stress beneath which delayed failure does not occur (Figure 2). This lower critical stress σ_a depends both on hydrogen concentration and root radius. In elastic-plastic deformation such as exists in the static loading tests on notched specimens, the longitudinal stress at the notch tip σ_{yy} is given by[26]

$$\sigma_{yy} = K_{\sigma(p)} \sigma_Y \tag{46}$$

where $K_{\sigma(p)}$ is the plastic stress concentration factor, and σ_Y is the tensile yield strength. Prior to cracking, $K_{\sigma(p)}$ increases with increasing plastic zone size,[63] and hence with decreasing rood radius ρ and increasing applied stress, σ, until it achieves a maximum value (2.57 for parallel sided cracks) that is dependent upon the included flank angle of the notch. Although general solutions of the variation of $K_{\sigma(p)}$ with σ are available only for bend loading,[64] some particular notch tension geometries have been worked out. Stiegerwald et al[39]

have used the solutions of Hendrickson et al[65] for a hyperbolic notch to show that for a particular hydrogen concentration the lower critical applied stress σ_a is that the stress at which the longitudinal stress below the notch σ_{yy} reaches a critical value σ_c, where σ_c = 355 ksi for specimens baked 3 hours at 300°F. This gives a value of $K_{\sigma(p)}$ = 1.69 for σ_Y = 210 ksi, and $K_{\sigma(p)}$ = 1.48 for σ_Y = 240 ksi. Consequently, the lower critical stress σ_a decreases as the yield strength is raised (e.g., by tempering at a lower temperature or by testing at a lower temperature) or as the root radius is decreased, since this allows $K_{\sigma(p)}$ to build up more rapidly with applied stress. They also noted that for a given geometry and value of σ_Y, σ_c and hence σ_a, decreased with increasing hydrogen concentration.

The existence of a critical local tensile stress for crack formation is consistent with recent theories of void growth,[45] which emphasize the importance of hydrostatic components in the process. Increasing hydrogen concentrations imply increasing hydrogen pressure inside the voids (or larger voids) and consequently lower longitudinal stresses at which they can coalesce to form a crack.

B. Slow Crack Growth in Hydrogenated Steels and Final Failure

Figure 12 indicates that slow crack growth occurs in discontinuous bursts once the incubation time has been exceeded. The time between bursts, t_b, is considerably smaller than the incubation time, t_i, indicating that the distance over which diffusion is occurring is smaller than that required for the diffusion of hydrogen to the crack before it began to grow. The microscopic processes leading to slow crack growth have been the subject of much conjecture. Troiano et al[21,37-39] postulate

that hydrogen atoms diffuse from the crack to positions in the iron lattice ahead of it which are subjected to high triaxial stress, and that embrittlement then results from the weakening of atomic bonds due to the presence of dissolved hydrogen. However, as stated previously, there is no evidence that hydrogen significantly affects the intrinsic strength of the iron crystal. Instead, it appears that the function of the hydrogen is to precipitate internally in microcrack and void nuclei (e.g., dislocation pile ups at particle interfaces) that are forming ahead of the advancing crack in regions of high triaxiality, building up pressure inside them. Since the nuclei are small, only a small amount of hydrogen needs to diffuse into them before the pressure inside them is a relatively large fraction of the pressure inside the crack, P_H. This diffusion raises the local stress available for void formation from $(\sigma_{yy} = K_{\sigma(p)}\ \sigma_Y)$ to $(\sigma_{yy} = K_{\sigma(p)}\ \sigma_Y + P_n)$. The stress required to form a void σ_G will vary statistically (Figure 14), since the particles responsible for void formation have varying sizes, shapes, interface strengths, etc.[26] However, for any distribution of values of σ_G, an increasing density of voids will be formed when hydrogen is present (Figure 14). These voids (Figure 15a) coalesce with each other, forming a microcrack (Figure 15b) which in turn coalesces with the advancing crack (Figure 15c) causing a burst of crack growth Δc. The process then repeats itself until the crack is sufficiently long to propagate unstably; this critical length depends on the applied stress and the value of G_c (Equation 11).

The rate of slow crack growth is limited by the diffusivity of hydrogen, since the hydrogen must diffuse into a void nucleus a distance

Δc from the crack tip. Suppose that all of the hydrogen which enters these voids comes from the advancing crack. Then in a time t_b, the maximum value of Δc is approximately $\sqrt{Dt_b}$. At room temperature, Steigerwald etal[62] noted bursts of crack growth at intervals, t_b, of about one minute. Taking $D \equiv 10^{-7} cm^2/sec$ for the diffusion of trapped hydrogen out of the crack into the nuclei gives $\Delta c \equiv 2.5 \times 10^{-3} cm$. This is of the order of the size ($10^{-3} cm$) of the individual microcracks that coalesce with the advancing crack, as shown in Figure 4 of reference 21. The rate of slow crack growth is $(\Delta c/t_b) = 4 \times 10^{-5} cm/sec$. This is in good agreement with reported values of the average rate of slow crack growth measured from the fracture surface of broken specimens, namely $1.4 \times 10^{-5} cm/sec$. As the temperature decreases, the time between bursts increases. From the data of Steigerwald et al it is possible to obtain approximate (because of the scatter) values of t_b at different temperatures and thereby determine the activation energy for the rate of slow crack growth. The value obtained in this manner, 7500 cal/gm mole, is in good agreement with the value of 7800 cal/gm mole for the diffusivity of trapped hydrogen (equation 31).

While it has been established that the average rate of slow crack growth decreases with decreasing hydrogen concentration,[21] there is no definite indication as to the dependence of growth rate on stress intensity factor. Except for the last burst that preceeds instability, it appears from the data shown in Figure 12 that the resistance increment that accompanies each burst is independent of time, hence independent of crack length and hence independent of K. On this basis, the failure time of charged specimens is given by equation (26), with A increasing

and t_i decreasing as the hydrogen content increases. Likewise, we would expect that A would increase as the yield strength increases (since this favors void formation[26]) and as the strain hardening rate decreases (since this favors void coalescence[45]), but these relations have not yet been established. However, it has been shown that for a given applied stress the time to failure does decrease as σ_Y increases.[70] While part of this decrease undoubtedly is due to a decrease in G_c with increasing σ_Y, some of it probably is due to increases in A and decreases in t_i.

The mode of hydrogen induced crack propagation in charged specimens is similar under uniaxial tensile loading. In unnotched specimens, fracture occurs well after general yield and, consequently, it is not possible to use the methods of linear elastic fracture mechanics to predict the failure stress or critical crack length. However, it is still apparent that the degree of hydrogen embrittlement will depend on the extent of hydrogen induced slow crack growth prior to instability. At very high strain rates, for example, hydrogen induced crack growth will not have time to occur before the material fails by the usual mode consistent with yield strength, temperature, etc. Hence the effect of hydrogen is minimal. Similarly, at very low temperatures the diffusivity of the hydrogen is too low to allow significant crack growth before failure. Again, therefore, hydrogen has little effect on ductility. The ductility of hydrogenated specimens of mild steel exhibits a minimum value somewhere below room temperature (depending on strain rate).[66] This results[26] from two competing effects. As the temperature increases, the increased rate of pressure build up in void nuclei ahead of the

advancing crack more than compensates for the decrease in σ_Y so that σ_{yy} increases and a larger number of voids and/or microcracks can be formed (Figure 14). However, the maximum hydrogen pressure in the void nuclei is limited by the pressure in the advancing crack and thus by the hydrogen content of the specimen. Consequently, as the temperature increases and σ_Y decreases, σ_{yy} will again decrease, fewer voids will form and coalesce, and the ductility will again increase.

These considerations indicate that since hydrogen causes embrittlement by producing an increase in the local stress field ahead of an advancing crack, as well as by helping to open the crack because of the pressure inside it, the same microstructural variables that increase ductility in the absence of hydrogen (e.g. fine grain size, spheroidal particles, and low inclusion content) will cause a smaller degree of embrittlement when hydrogen is present.[20,67]

Alloy composition has little direct effect on a steel's susceptibility to hydrogen embrittelement, in the sense that there is no one element that strongly increases or decreases susceptibility. However, it has been shown[25] that additions of silicon and chromium reduce the diffusivity of hydrogen in steel, and consequently their presence would be expected to reduce the rate of slow crack growth. The yield strength of the steel is an important factor and, as in the case of brittle fracture in the absence of hydrogen, the severity of embrittlement increases with strength (Figure 1). Since changes in strength can be achieved by changes in alloy composition as well as by variations in heat treatment, alloy composition can have an indirect effect on the degree of hydrogen embrittlement.

V. HYDROGEN EMBRITTLEMENT IN AN EXTERNAL HYDROGEN ENVIRONMENT

In addition to the hydrogen embrittlement that occurs when a large concentration of excess hydrogen is initially present inside the metal (e.g., in electroplated or rapidly solidified structures), there is also the embrittlement that can occur when hydrogen from an external environment is present during all stages of crack initiation and growth. Hydrogen embrittlement during corrosion is one example of this type of embrittlement. From a microscopic point of view, the embrittlement mechanism should be similar to that described in Sections III and IV, since the fugacity of the liberated hydrogen will be high enough to cause void formation and coalescence ahead of the advancing crack tip. One difference should be noted; namely, that since the faces of the growing crack are directly exposed to the external environment, there is a ready and constant supply of hydrogen available for crack growth. This could lead to a smaller value of the incubation time, t_i, and a faster rate of slow crack growth as compared with cathodically charged specimens.

It is extremely difficult to determine whether fracture in some corrosive environments was the result of hydrogen embrittlement or stress corrosion cracking, since the fracture surfaces exhibit many similar features, even when observed by electron microscopy. In high strength steels, both modes of failure are predominantly intergranular.[71] Careful examination by electron microscopy has revealed that stress corrosion cracking nucleates at the surface, whereas hydrogen corrosion embrittlement nucleates beneath the surface. Furthermore, the fracture surfaces resulting from stress corrosion cracking tend to be smoother and exhibit fewer hairline cracks, than those resulting from hydrogen

embrittlement. Since corrosion products tend to obscure the detail in both cases, the exact analysis in all situations would be extremely difficult.

One simpler method of separating the two forms of embrittlement in testing is to note the effect of small impressed currents on the time to fail in a static test[10] or upon the rate of crack growth.[14] If the presence of a small cathodic current reduces embrittlement (Figure 16a) the fracture process in the absence of the imposed current is due to stress corrosion cracking. However, when anodic currents reduce the embrittlement (Figure 16b) the normal fracture process in the particular environment is hydrogen embrittlement. While large impressed anodic currents are also able to reduce the degree of hydrogen embrittlement, they may in turn cause stress corrosion cracking and vice-versa. Therefore, the degree of cathodic or anodic protection given to a particular structure operating in a particular environment must be carefully controlled.

Recent investigations[12,14] indicate that the rate of slow crack growth in high strength steel immersed in distilled water or water vapor increases with increasing temperature and increasing stress intensity factor. However, conflicting data on the kinetics of growth have been reported. Vanden Sluys[14] found that the rate of slow crack growth in 4340 steel (σ_Y = 215 ksi) is given by

$$\frac{dc}{dt} = \lambda\, e^{-\Delta H/RT} \tag{47}$$

where the activation energy ΔH decreases with increasing stress intensity factor. His data show that

$$\Delta H = \Delta H_o - BK \tag{48}$$

so that

$$\frac{dc}{dt} = \lambda\, e^{-\Delta H_o/RT}\quad e^{BK/RT} \tag{49}$$

where $\lambda = 7.5 \times 10^4$ in/min., $\Delta H_o = 9150$ cal/gm mole and B = 30 cal/1 ksi $\text{in.}^{\frac{1}{2}}$. The dependence of dc/dt upon K is shown in Figure 17, where it is noted that the rate of crack growth is finite at k = 0 (i.e., crack growth could occur in the absence of applied stress). When BK is small compared to RT the exponential can be expanded as $e^x \simeq 1 + x$ so that

$$\frac{dc}{dt} = \lambda\, e^{-\Delta H_o/RT}\left[1 + \frac{BK}{RT}\right] \tag{50}$$

and a linear dependence of (dc/dt) upon K is found.

Johnson and Wilner[12] also noted that dc/dt was linearly proportional to K, and that crack growth was thermally activated with $\Delta H \approx 9000$ cal/gm mole in H-11 steel (σ_Y = 230 ksi). Their data, however, indicate a much stronger dependence on K, Figure 17, and furthermore that dc/dt = 0 at a limiting value of $K = K^*_I$. At ambient temperature, 100% relative humidity, K^*_I = 18 ksi $\text{in.}^{\frac{1}{2}}$. K^*_I is then the analog of the parameter K_{ISCC}, below which stress corrosion cracking will not take place. The linear dependence of (dc/dt) upon K means that equation (27) can be used to predict the failure time under static loading, with $t_i = 0$ and K replaced by $(K-K^*_I)$. These workers also observed that in humidified argon the rate of slow crack growth decreased, and K^*_I increased as the relative humidity of the atmosphere decreased (Figure 8). They were not able to conclude from their results whether hydrogen embrittlement or stress corrosion cracking was responsible for the slow crack growth, since a value of ΔH = 9 kcal/mole is consistent with either the

diffusion of hydrogen in iron or, in their opinion, the diffusion of oxygen in water. This suggests the need for measurements of the temperature sensitivity of stress corrosion cracking to determine the activation energy for the process, and thereby to compare it with values obtained in ambiguous situations such as described here.

In addition to the embrittlement which occurs in corrosive liquids and in the presence of a cathodic "protection" system, it has also been shown that embrittlement in high strength steels can occur in the presence of hydrogen gas.[13,15-19] Slow crack growth has been noted at hydrogen pressures as low as one atmosphere,[13] provided that oxygen is absent but in general the embrittlement is more pronounced at higher pressures (2000-10,000 psi). Also the embrittlement is more pronounced as the strength level of the steel increases. Since the maximum pressure that can build up inside a void is of the order of the external pressure, it is unlikely that the embrittlement is due to pressure build up inside the voids, as in the case of cathodically charged or corroded specimens. Instead, it appears that the primary function of the hydrogen is to absorb preferentially in place of oxygen[13] and promote embrittlement by removing the oxide layer.+

The effect of small oxygen additions on retarding the rate of slow crack growth in an H-11 steel is shown in Figure 18. Similarly, it has been suggested[13] that embrittlement in water and water vapor described above may result from the dissolution of protective oxide coatings in the presence of H_2O.

The importance of an oxide film in retarding slow crack growth, and hence the importance of hydrogen in preventing film formation, is open

to speculation. Since crack growth involves the coalescence of a void with the crack tip, the plastic processes taking place in the vicinity of the tip would be expected to play a large role in determining the crack opening displacement required for incremented growth. It is known, for example, that oxide layers, even on laboratory size tensile specimens, can increase the rate of strain hardening,[68,69] probably by blocking the exit of dislocations and causing the formation of pile up dislocation groups. These layers would probably produce even larger effects on the volume element that is necking down at the crack tip. If removal of the layer results in a decreased local rate of strain hardening, the local plastic flow becomes much more inhomogeneous and coalescence would occur at smaller crack tip displacements.

VI. SUMMARY

The process of brittle fracture in structural materials can be separated into three stages; 1) crack nucleation, 2) slow crack growth, and 3) rapid, unstable fracture. Hydrogen embrittles steel by affecting the first two of these stages. In corroded, electrolytically charged, or thermally charged specimens, excess hydrogen precipitates at inclusions or carbides in molecular form, causing the initiation of voids or microcracks. The hydrogen pressure in these defects causes them to grow either by plastic deformation or by cleavage, depending on the intrinsic toughness of the particular steel and the shape of the nucleating particle. It is shown that the size of the defects is determined by the spacing of the nucleating particles. Consequently, small voids or cracks will exist when a given volume of second phase is finely distributed. In hot rolled materials, alignment of inclusions can be used to minimize

hydrogen embrittlement.

Microcrack or void coalescence, to form a macrocrack, occurs when a stress is applied to a hydrogenated structure. The effect of hydrogen concentration, applied stress, notch geometry, strength level, temperature, and microstructure on the incubation time for slow crack growth, the rate of slow crack growth, and the time to fail in a static test or the tensile ductility are considered. Finally, crack growth in external environments, such as hydrogen gas is also discussed briefly.

ACKNOWLEDGEMENTS

The author wishes to thank Professor G. M. Pound for helpful discussions during the preparation of this report and the National Aeronautics and Space Agency for support on Grant NSG-622.

FOOTNOTES

Page 17. + Neglecting the equilibrium concentration C_{eq} as being small compared to C_H.

Page 22. +Note: To prevent outgassing during testing at room temperature static loading tests are either performed in an electrolytic bath, with hydrogen continually introduced during testing, or on specimens that have been cadmium plated after charging.

Page 31. +Based on its high heat of adsorption, oxygen would be expected to adsorb in place of hydrogen at equivalent partial pressures of the two gases, forming an oxide, provided reduction of the oxide did not occur.

REFERENCES

1. Scheutz, A. E., and Robertson, W.D., Corrosion, 13:437 (1957).
2. Sachs, G., WADC Report TR53-254 (1954).
3. Vlannes, P.N., Strauss, S. W., and Brown, B.F., NRL Rept 4906 (1957).
4. Geyer, N.M., Lawless, G.W., Cohen, B., "Hydrogen Embrittlement in Metal Finishing", p 109, Reinhold, New York (1961).
5. Sully, A. H., and Bell, W. A., J. Iron Steel Inst., 178:15 (1954).
6. Andrew, J.H., Lee, H., Malik, A. K., and Quarrell, A.G., J. Iron and Steel Inst., 153:67 (1946).
7. Biggs, W.D., "Brittle Fracture of Steel", p 333, MacDonald and Evans, London (1960).
8. Smialowski, M., "Hydrogen in Steel", Addison-Wesley, Reading, Mass. (1962).
9. Baker, R.G. and Watkinson, F., Hydrogen in Steel, BISRA Rept. 73, (1962), p 123.
10. Brown, B. F., NRL Rept 6041 (November 1963).
11. Hanna, G. L., Troiano, A.R., and Steigerwald, E.A., Trans ASM, 57:658, (1961).
12. Johnson, H. H. and Wilner, A.M., App. Matls Res. p 34 (January 1965).
13. Hancock, G. G., and Johnson, H. H., Trans AIME, 236:513 (1966).
14. Sluys, Van der, W. A., University of Illinois, TAM Rept 292, (1966).
15. Hofmann, W., and Rauls, W., Weld. J. Res. Supp, 255A (1965)
16. Cavett, R. A. and Van Ness, H.C., Weld. J. Res. Supp, p 316 (1963).
17. Williams, D., and Nelson, H., To be published.
18. Walter, R.J., Chandler, W.T., Rocketdyne Research Rept #R6851 (January 1967).

19. Steinman, J. B., Van Ness, H. C., and Ansell, G. S., Weld J., 44:221s (1965).

20. Bastien, P., "Physical Metallurgy of Stress Corrosion Fracture", p 311, Interscience, New York (1959).

21. Troiano, A., Trans ASM, 52:54 (1960).

22. Cottrell, P. P., Prog. in Mat. Sci., 9: No 4:201 (1961).

23. Tetelman, A. S., "Fracture of Solids", p 671, Interscience, New York (1963).

24. Farrell, K., and Quarrell, A. G., J. Iron Steel Inst., 202:1002 (1964).

25. Fletcher, E. E., Berry, W. E., and Elsea, G. A., DMIC Report #232 (1966).

26. Tetelman, A. S., and McEvily, A. J., "Fracture of Structural Materials", Wiley, New York (1967).

27. Zapffe, C., and Sims, C., Trans. AIME, 145:225 (1941).

28. de Kazinsky, F. J., J. Iron Steel Inst., 177:85 (1954).

29. Garafolo, F., Chow, Y., Ambegaokar, R., Acta Met., 8:504 (1960).

30. Bilby, B. A., and Hewitt, J., Acta Met., 10:587 (1962).

31. Tetelman, A. S., and Robertson, W. D., Trans AIME., 224:775 (1962).

32. Tetelman, A. S., and Robertson, W. D., Acta Met., 11:415 (1963)

33. Petch, N. O., Staples, Nature, 169:842 (1952)

34. Tetelman, A. S., Wagner, C. N. J., Robertson, W. D. Acta Met., 9:205 (1961).

35. Hill, M. L. and Johnson, E. W., Trans. AIME, 215:717 (1959).

36. Fayet, A., M. S. Thesis, Stanford University (1966).

37. Morlet, J. G., Johnson, H. H., Troiano, A. R., JISI, 189:37 (1958).

38. Johnson, H. H., Morlet, J. G. and Troiano, A. R., Trans. Aime, 212:526 (1958).

39. Steigerwald, E. A., Schaller, F. W., and Troiano, A. R., Trans. AIME 212:832 (1960).

40. Cottrell, A. H., "Fracture" p 1, Wiley, New York (1959).

41. Hahn, G. T., Averbach, B.L., Owen, W. S., and Cohen, Morris, "Fracture", p 91, Wiley, New York (1959).

42. McMahon, C. J., Ship. Struc. Comm. Rept SCC-161 (1964).

43. Kaechle, L., and Tetelman, A. S., To be published.

44. McClintock, F. A., J. Appl. Mech., 25:282 (1958).

45. McClintock, F. A., To be published.

46. Wells, A. A., Brit. Weld, Jour. p 855 (1963).

47. Hahn, G. T., and Rosenfield, A., Acta Met. 13:293 (1965).

48. Cottrell, A. H., Proc. Roy. Soc., 285:10 (1965).

49. Bilby, B. A., Cottrell, A. H. and Swinden, K. H., Proc. Roy. Soc., 272:304 (1963).

50. McClintock, F. A. and Irwin, G. R., Fracture Toughness Testing, ASTM, Philadelphia, STP No. 381 (1965) p. 84.

51. Knott, J. F., J. Iron Steel Inst., 204:1014 (1966).

52. Irwin, G. R., Encl of Physics, Vol. Vl, Springer, Heidelberg (1958).

53. Paris, P.C., and Sih, G.C.M., Fracture Toughness Testing, ASTM, Philadelphia, STP. No. 381 (1965), p 30.

54. McEvily, A. J., and Bond, A. P., J. Electrochem. Soc., 112:131 (1956).

55. Geller, W. and Sun, T., Arch, Eisenhutt 21:437 (1950).

56. Carslaw, H.S., and Jaeger, J.C., "Conduction of Heat in Solids", Oxford (1959).

57. Tetelman, A. S., D. Eng. Thesis, Yale University (1961).

58. Churchman, A. T., Barnes, R. S., and Cottrell, A. H., J. Nuc. Eng. 2:88 (1958).

59. Tetelman, A. S., and Johnston, T. L., Phil. Mag., 11:389 (1965).

60. Gell, M., Briant, J. P. and Robertson, W. D., Trans AIME, 239, 813 (1967).

61. Barnett, W. J. and Troiano, A. R., Trans. AIME, 209:486 (1957)

62. Steigerwald, E. A., Schaller, F. and Troiano, A., Trans. AIME, 215:1048 (1959)

63. Wilshaw, T. R., and Pratt, P. L., J. Mech. Phys. Solids, 14:7 (1966).

64. Wilshaw, T. R., Rau, C. A., and Tetelman, A. S., To be published in Proceedings of National Symposium on Fracture Mechanics, Held at Lehigh University (June 1967).

65. Hendrickson, J. A., Wood, D. S., Clark, D. S., Trans. ASM 50:656 (1958).

66. Toh, T., and Baldwin, W. M., "Stress Corrosion Cracking and Embrittlement" p 176, Wiley, New York (1956).

67. Petch, N. J., Phil. Mag., 1:331 (1956).

68. Kramer, I. R., Trans. AIME, 227:1003 (1963).

69. Nelson, H., Williams, D., "Env. Sens. Mech. Behavior of Materials". p. 107, Gordon & Breach (1967).

70. Frohmberg, R. P., Barnett, W. J., and Troiano, A. R., Trans. ASM 47:892 (1955)

71. Geuss, E., Surface Science, 2:48 (1964).

FIGURE CAPTIONS

1. The effect of hydrogen content on the tensile ductility of high strength steel.[24]

2. Schematic diagram of the effect of applied stress on the incubation time for slow crack growth and the time to fracture for notched tensile specimens of hydrogenated high strength steel.[21]

3. Microcrack produced in iron-3% silicon by the cathodic charging of hydrogen, in the absence of applied stress. Strain pattern around crack revealed by dislocation etch pitting.[31]

4. a) Void formation at strain $\epsilon = \epsilon_1$, b) elongation of voids at $\epsilon_2 > \epsilon_1$, and c) coalescence of voids to form a crack at $\epsilon_3 > \epsilon_2$.

5. The variation of crack length with applied stress. a) Unstable fracture initiated at a stress $\sigma = \sigma_F$, without prior slow growth of crack of length $2c_o = 2c_F$. b) Slow crack growth from c_o to c_F occurs before unstable fracture at $\sigma = \sigma_F$. c) Slow crack grwoth begins at time $t = t_i$ under constant stress; unstable fracture occurs when $c = c_F$ at time $t = t_F$.[26]

6. Effect of temperature on the Charpy V notch impact energy for low strength ($\sigma_Y < \frac{E}{300}$) and high strength ($\sigma_Y > \frac{E}{150}$) steels.

7. Profile of fracture surface due to rupture. A high void density leads to a brittle rupture (small crack opening displacement) whereas a low void density leads to a tough rupture (large crack opening displacement).

8. Effect of stress intensity factor K and humidity level on the rate of slow crack growth in H-11 steel in humidified argon.[12]

9. Schematic diagram of the lattice hydrogen concentration immediately

after excess hydrogen has been introduced (initial condition) and after some diffusion has occurred to the growing void. C_{eq} is the equilibrium concentration, according to equation (29).

10. Diffusion of excess hydrogen to growing void. Essentially all hydrogen atoms within a distance r* from a growing void will go to that particular void rather than to another.

11. Microcrack nucleus formed by dislocation pile up ahead of an advancing crack. Crack grows by joining with nucleus.[59]

12. The electrical resistance increase as a function of time for hydrogenated notched tensile specimen of 4340 steel, tested at an applied stress of 180 ksi at 0°F.[62]

13. Variation of incubation time with applied stress and hydrogen concentration; the latter was varied by baking for different times at 300°F after charging.[38]

14. The fraction of grains that crack, or voids that form, at a particular tensile stress level σ_G; shaded area is the total fraction of voids that form, or grains that crack, when $\sigma = \sigma_G$. The presence of a hydrogen pressure P_n increases the density of voids and/or fractured grains ahead of an advancing crack, by increasing the local tensile stress level.[26]

15. Process of slow crack growth in notched tensile specimens. a) Void formation ahead of crack, b) void coalescence, c) coalescence of large void with crack, causing crack tip to advance a distance Δc.

16. Effect of impressed currents on time to fail of martensitic steel in a) H_2S solution and b) acetic acid solution containing a sulfide poison.[10]

17. Effect of stress intensity factor K on the rate of slow crack growth of 4340 steel in water[14] and H-11 steel in 100% humidified argon[12] at 80°F.

18. Slow crack growth in H-11 steel in hydrogen and a hydrogen-oxygen mixture.[13]

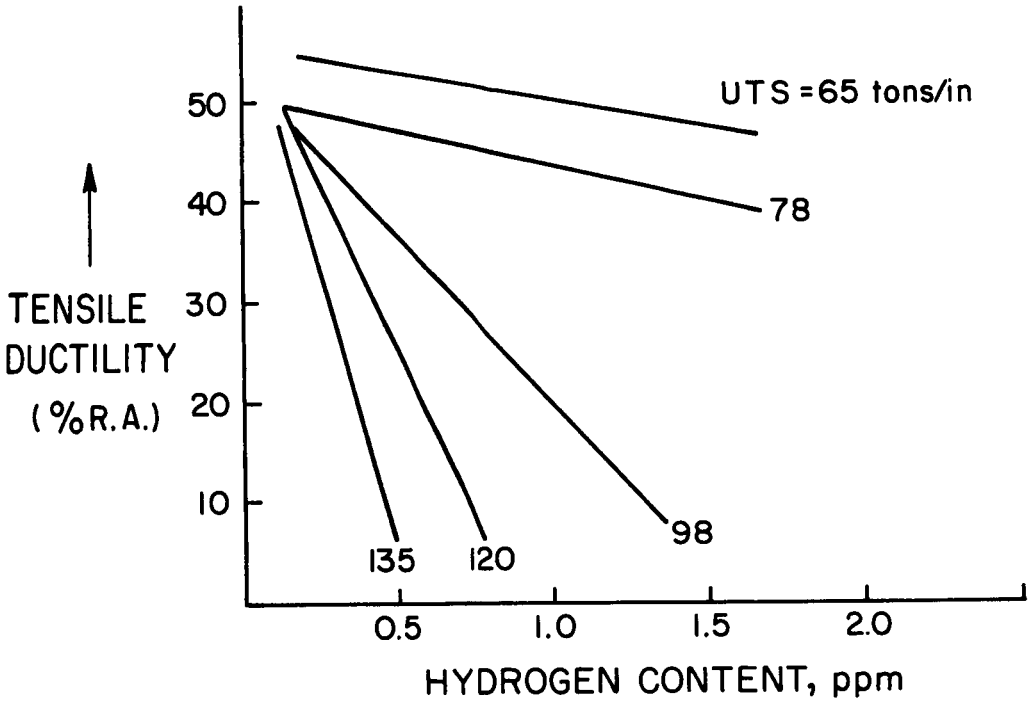
UTS =65 tons/in
78
98
120
135
50
40
30
20
10
TENSILE
DUCTILITY
(%R.A.)
0.5
1.0
1.5
2.0
HYDROGEN CONTENT, ppm

FIGURE 1

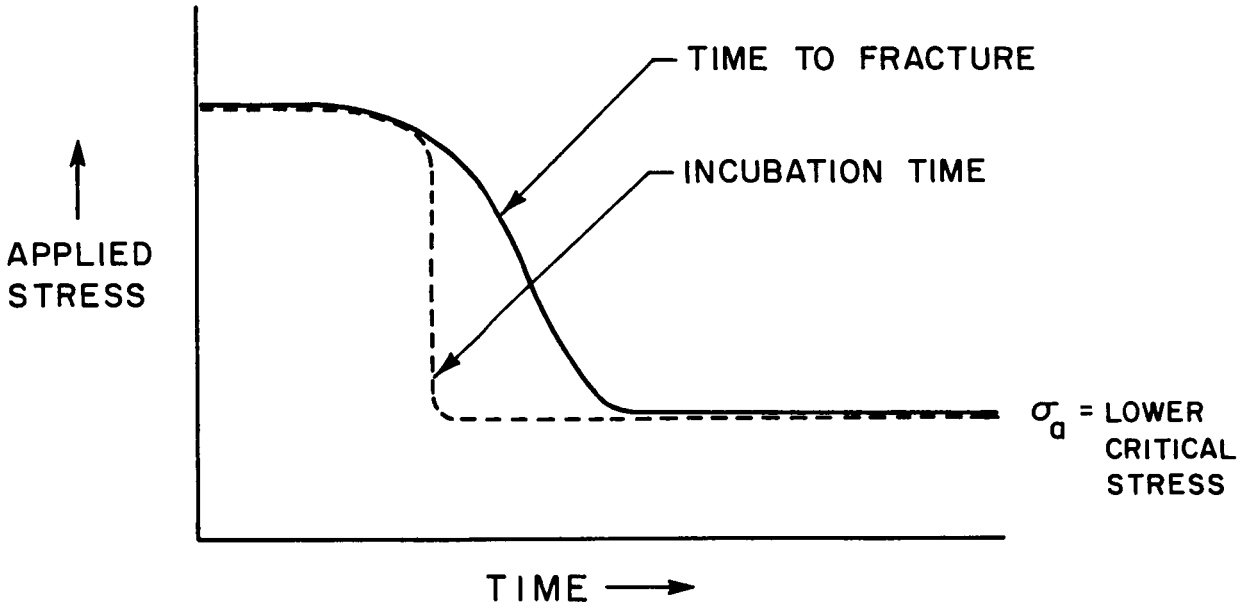
TIME TO FRACTURE
INCUBATION TIME
APPLIED STRESS
σ_a = LOWER CRITICAL STRESS
TIME

FIGURE 2

FIGURE 3

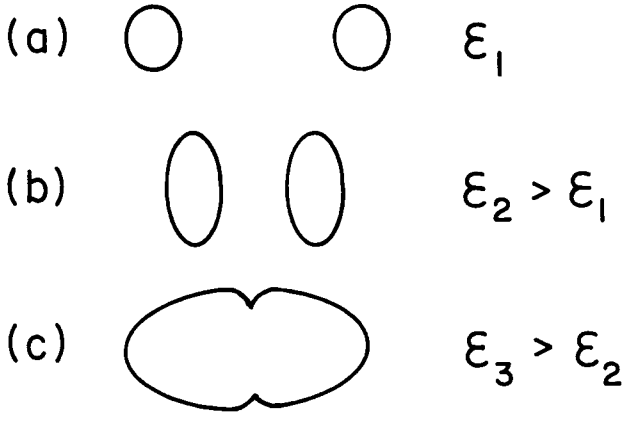
(a)
ε_1
(b)
$\varepsilon_2 > \varepsilon_1$
(c)
$\varepsilon_3 > \varepsilon_2$

FIGURE 4

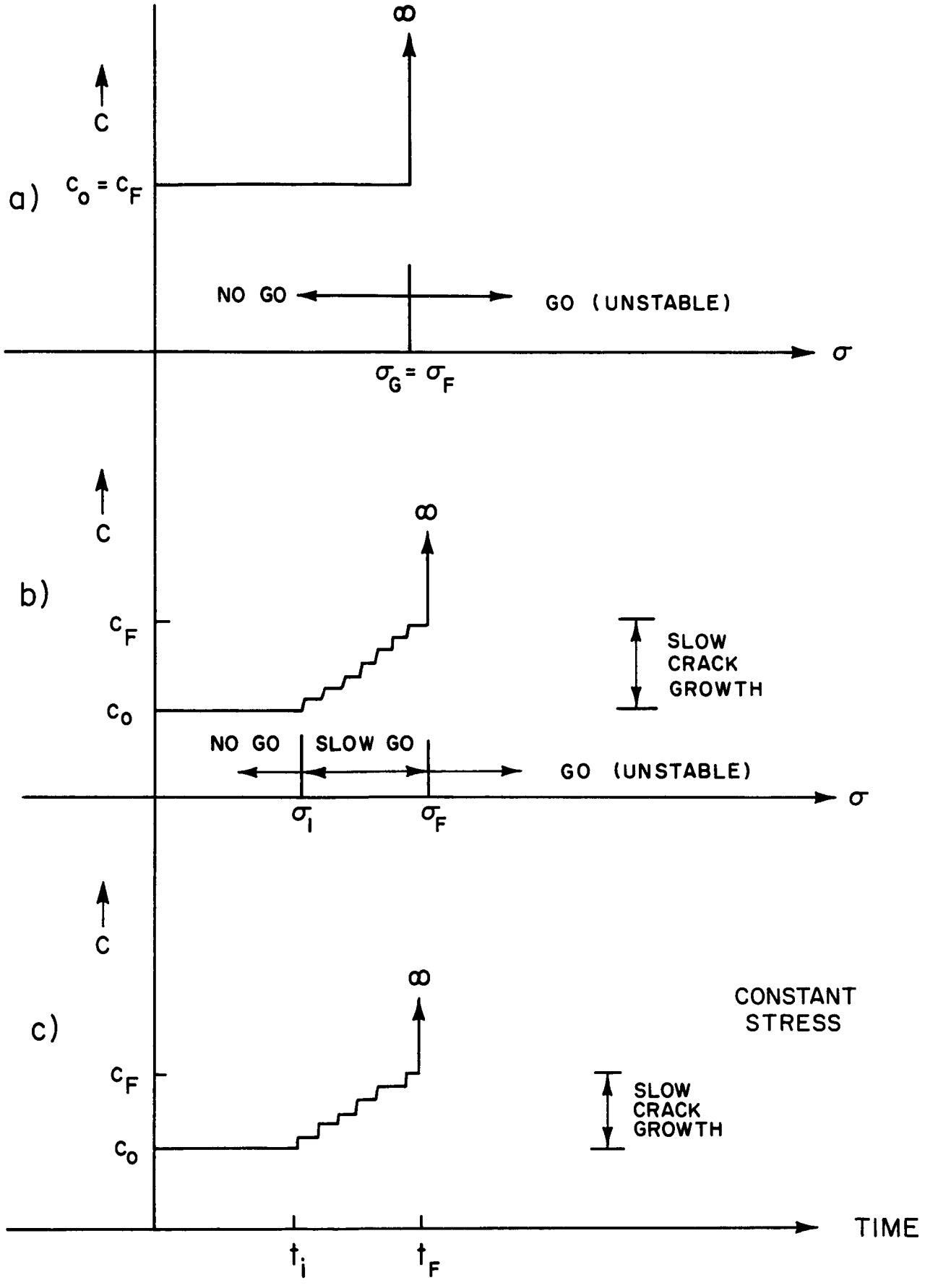
∞
C
a)
$c_o = c_F$
NO GO
GO (UNSTABLE)
σ
$\sigma_G = \sigma_F$
C
∞
b)
c_F
c_o
SLOW
CRACK
GROWTH
NO GO
SLOW GO
GO (UNSTABLE)
σ
σ_i
σ_F
C
∞
CONSTANT
STRESS
c)
c_F
c_o
SLOW
CRACK
GROWTH
TIME
t_i
t_F

FIGURE 5

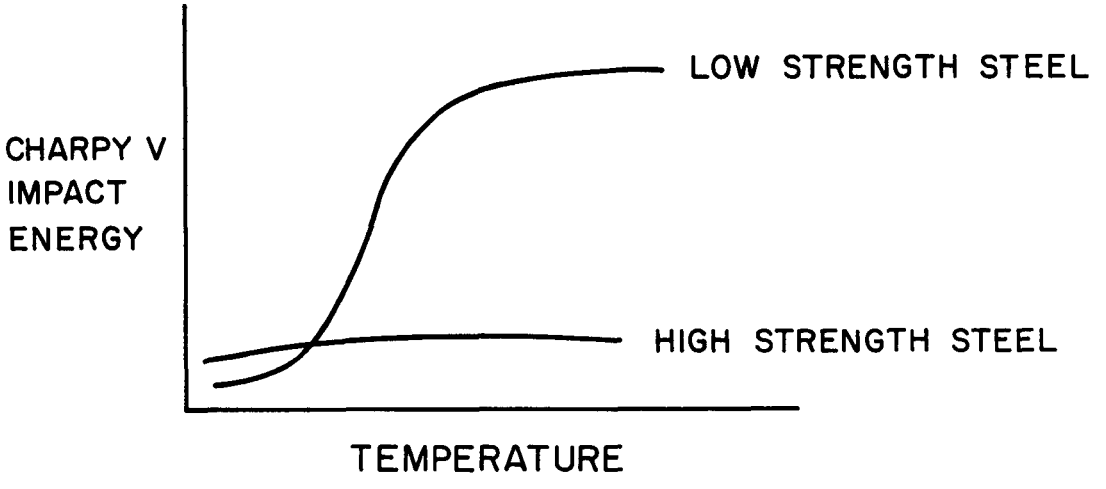
LOW STRENGTH STEEL
CHARPY V
IMPACT
ENERGY
HIGH STRENGTH STEEL
TEMPERATURE

FIGURE 6

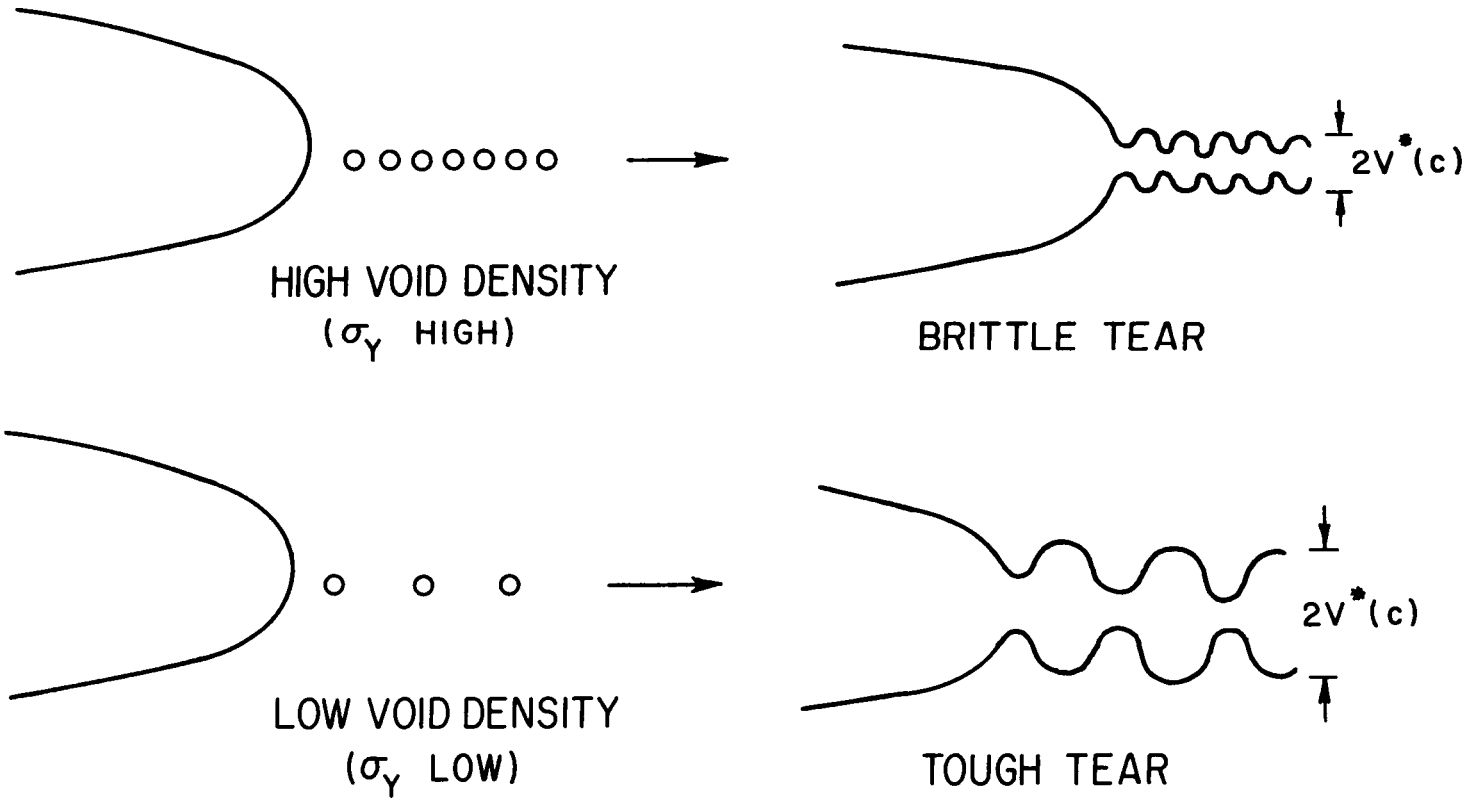
HIGH VOID DENSITY
(σ_Y HIGH)
BRITTLE TEAR
$2V^*(c)$
LOW VOID DENSITY
(σ_Y LOW)
TOUGH TEAR
$2V^*(c)$

FIGURE 7

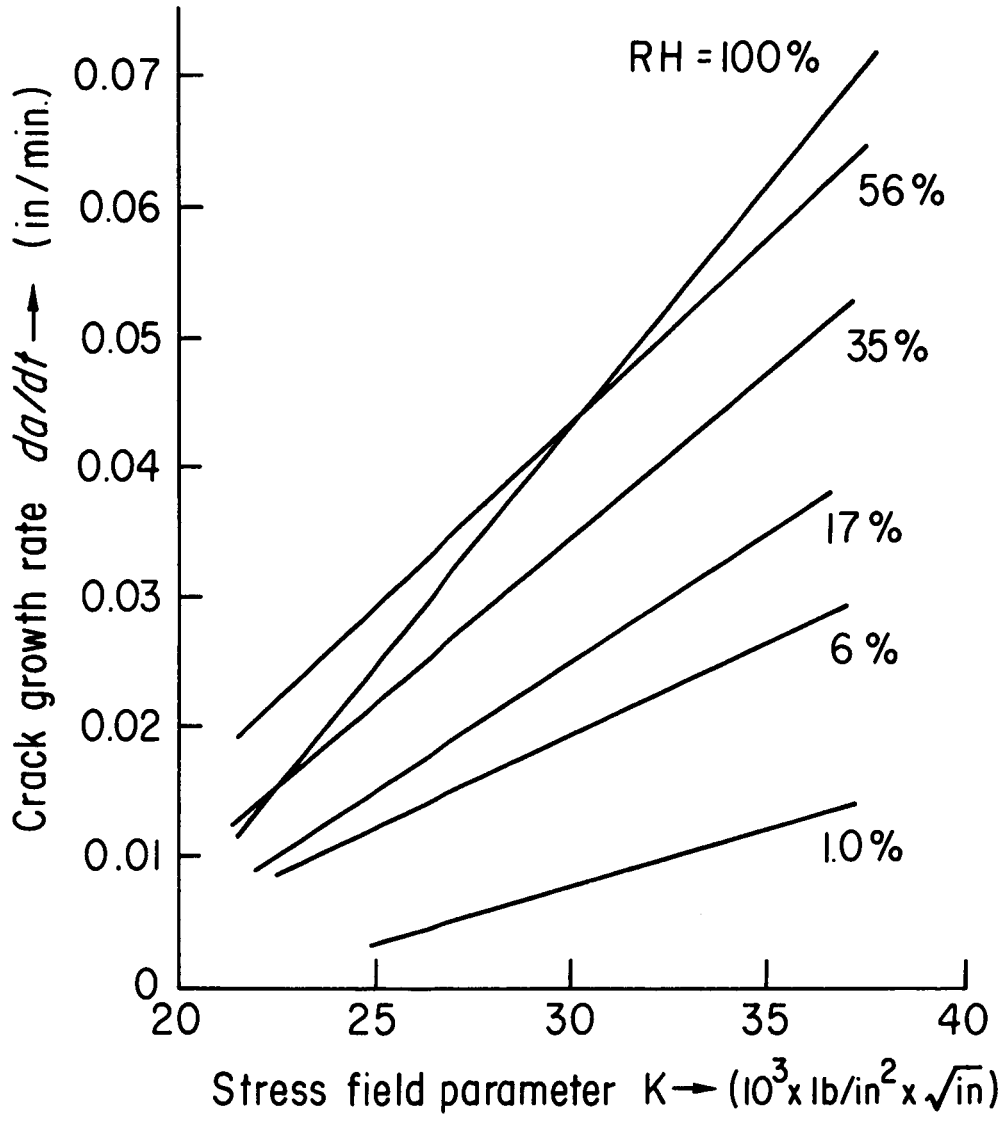
RH = 100%
56%
35%
17%
6%
1.0%
0.07
0.06
0.05
0.04
0.03
0.02
0.01
0
20
25
30
35
40
Crack growth rate da/dt → (in/min.)
Stress field parameter K → (10³ x lb/in² x √in)

FIGURE 8

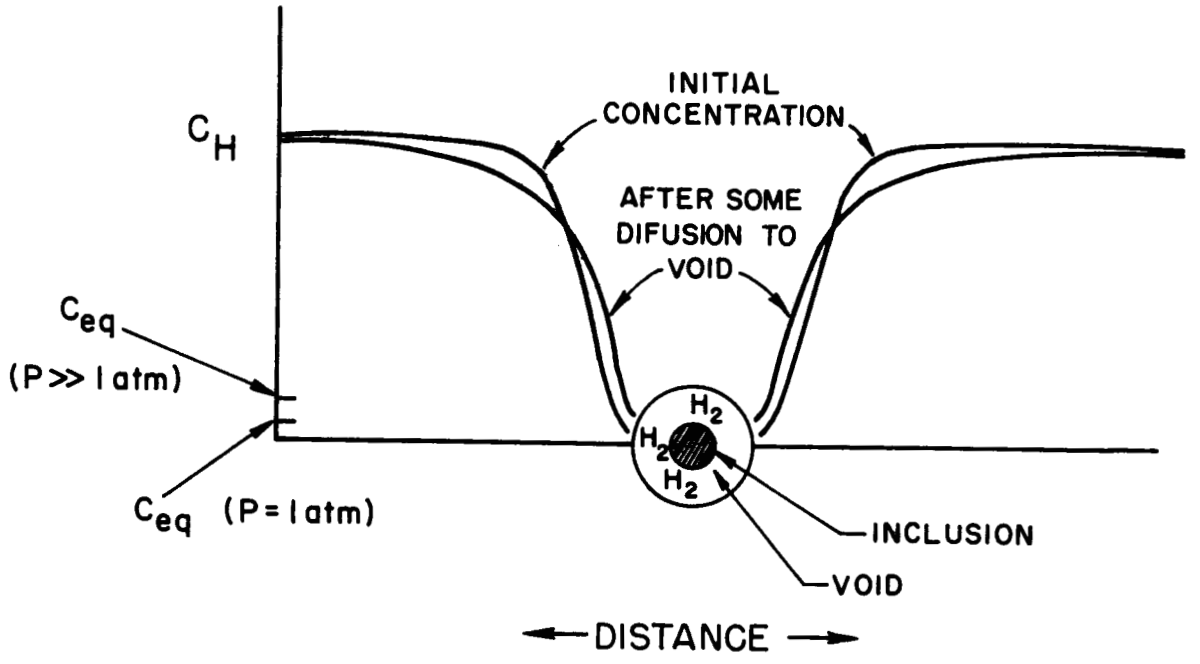
C_H
INITIAL CONCENTRATION
AFTER SOME DIFUSION TO VOID
C_{eq}
(P >> 1 atm)
C_{eq} (P = 1 atm)
H_2
H_2
H_2
INCLUSION
VOID
DISTANCE

FIGURE 9

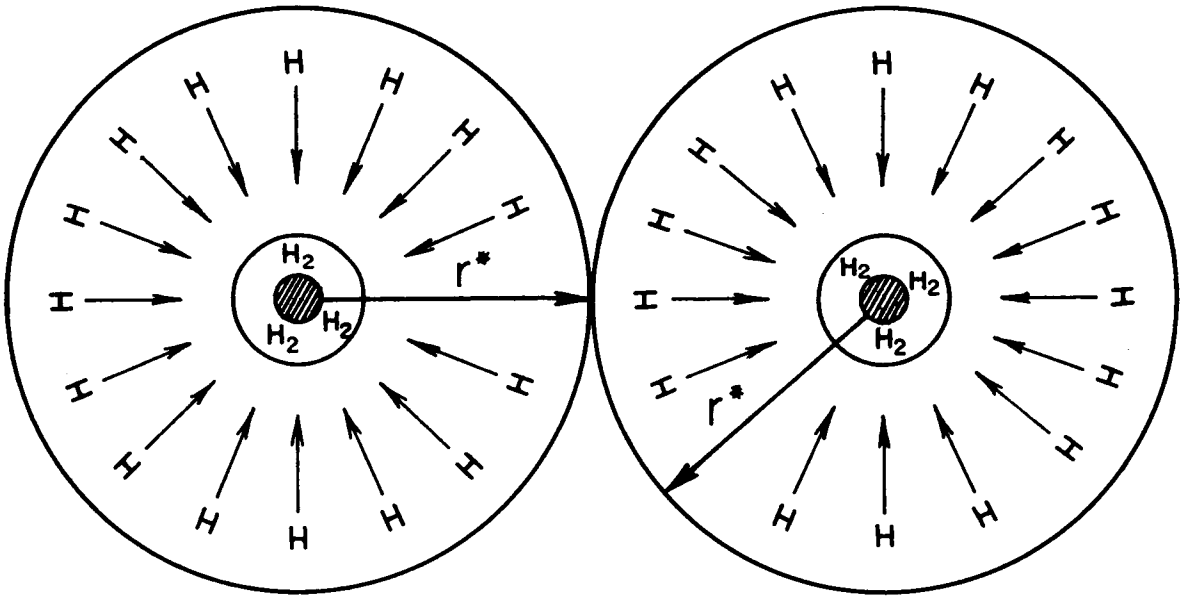

FIGURE 10

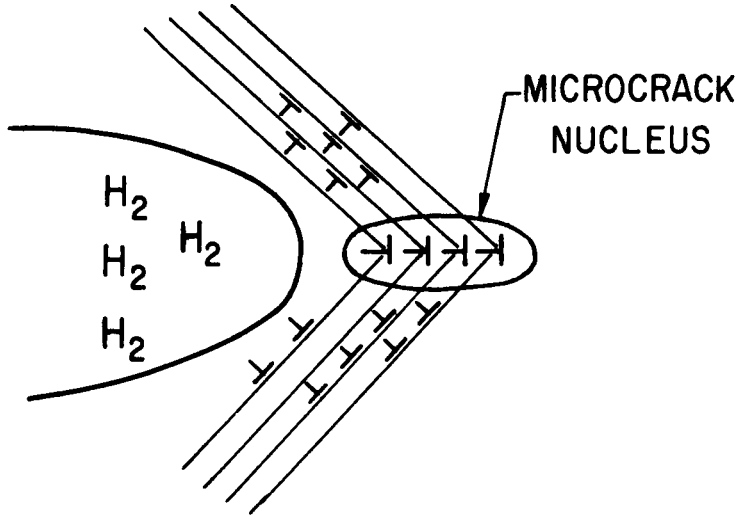

FIGURE 11

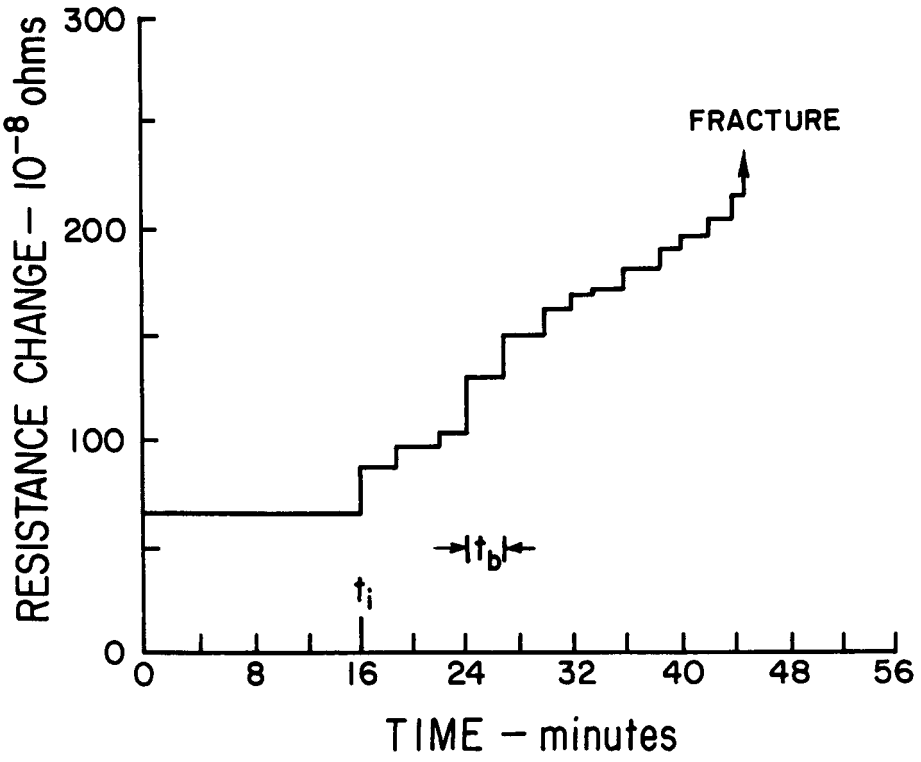
RESISTANCE CHANGE – 10^{-8} ohms
300
200
100
0
FRACTURE
t_b
t_i
0
8
16
24
32
40
48
56
TIME – minutes

FIGURE 12

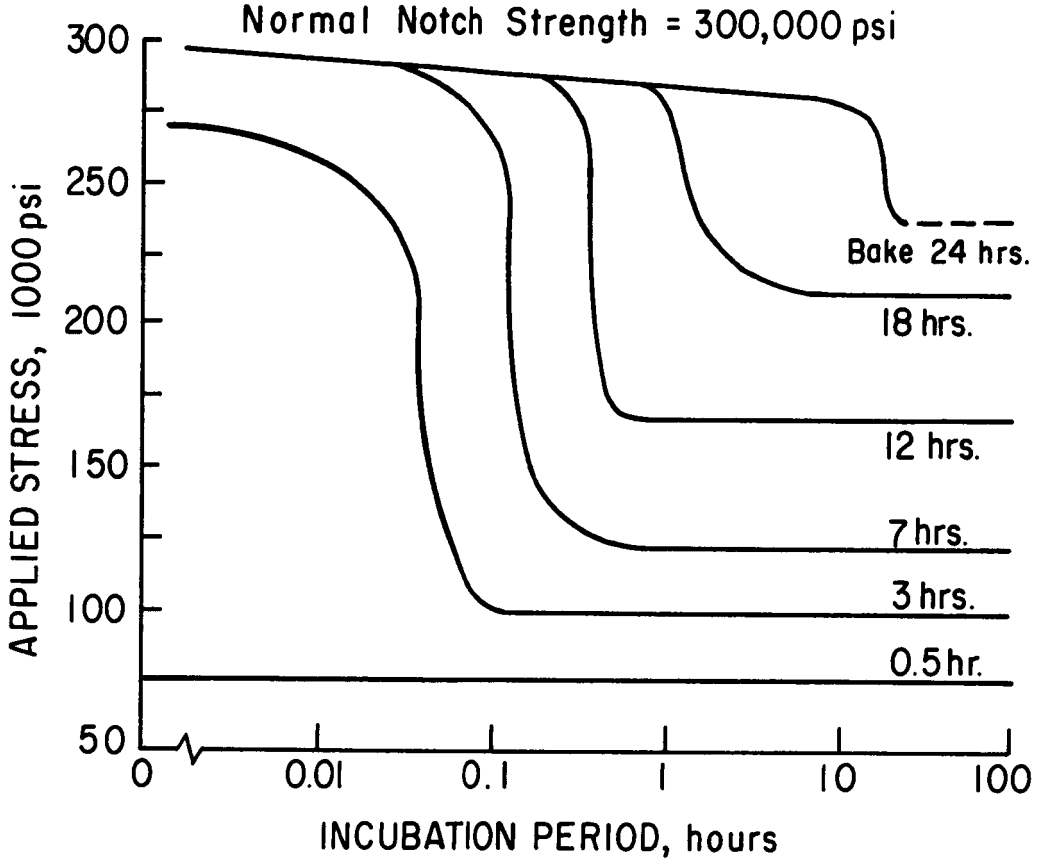
Normal Notch Strength = 300,000 psi
300
250
200
150
100
50
APPLIED STRESS, 1000 psi
Bake 24 hrs.
18 hrs.
12 hrs.
7 hrs.
3 hrs.
0.5 hr.
0
0.01
0.1
1
10
100
INCUBATION PERIOD, hours

FIGURE 13

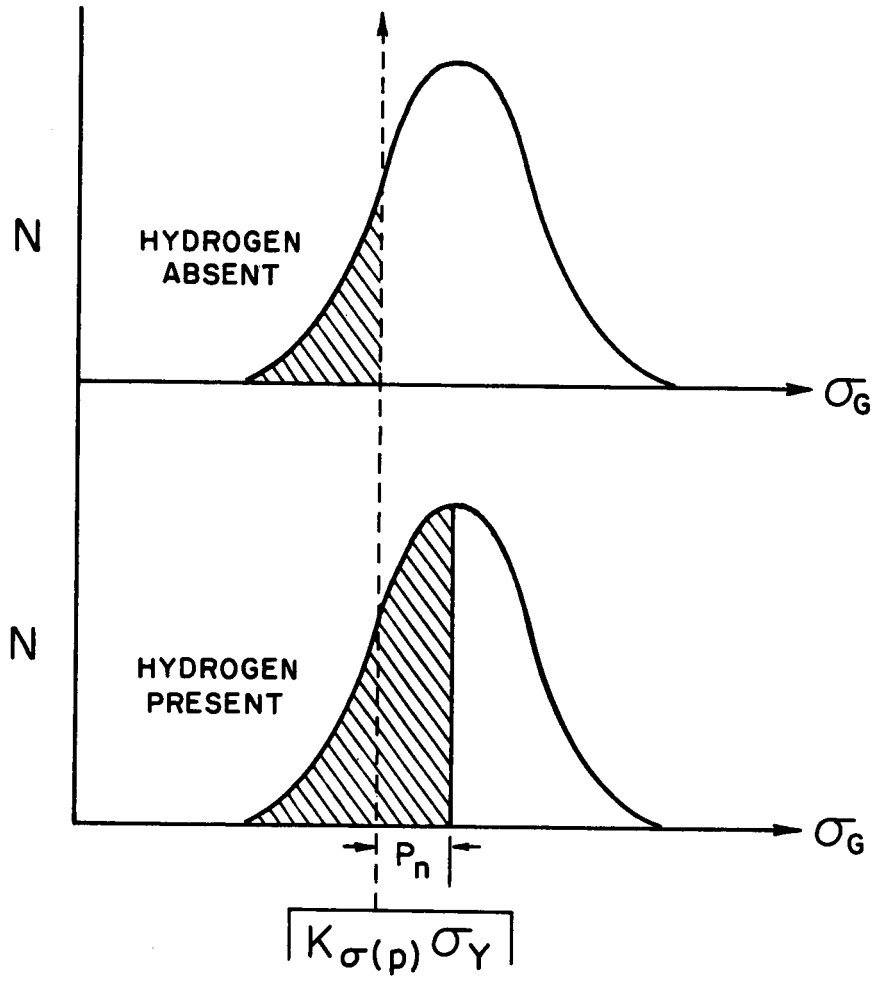
N
HYDROGEN
ABSENT
σ_G
N
HYDROGEN
PRESENT
σ_G
P_n
$K_{\sigma(p)}\sigma_Y$

FIGURE 14

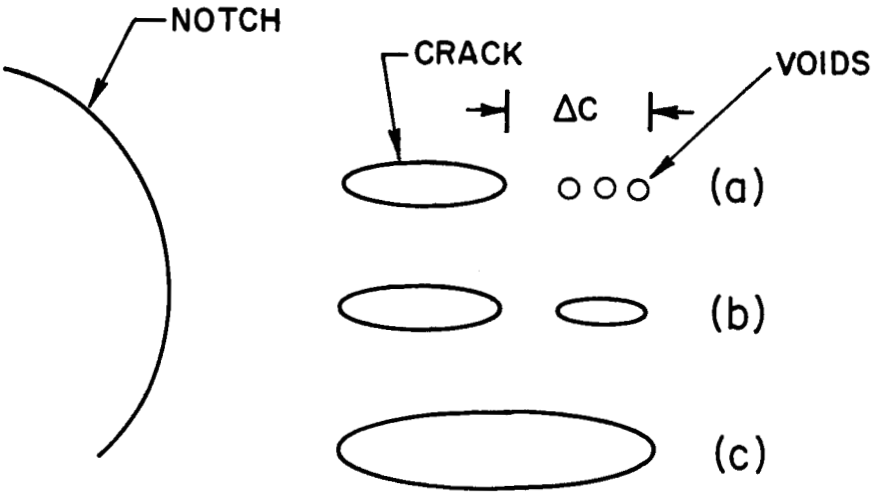

FIGURE 15

(a)

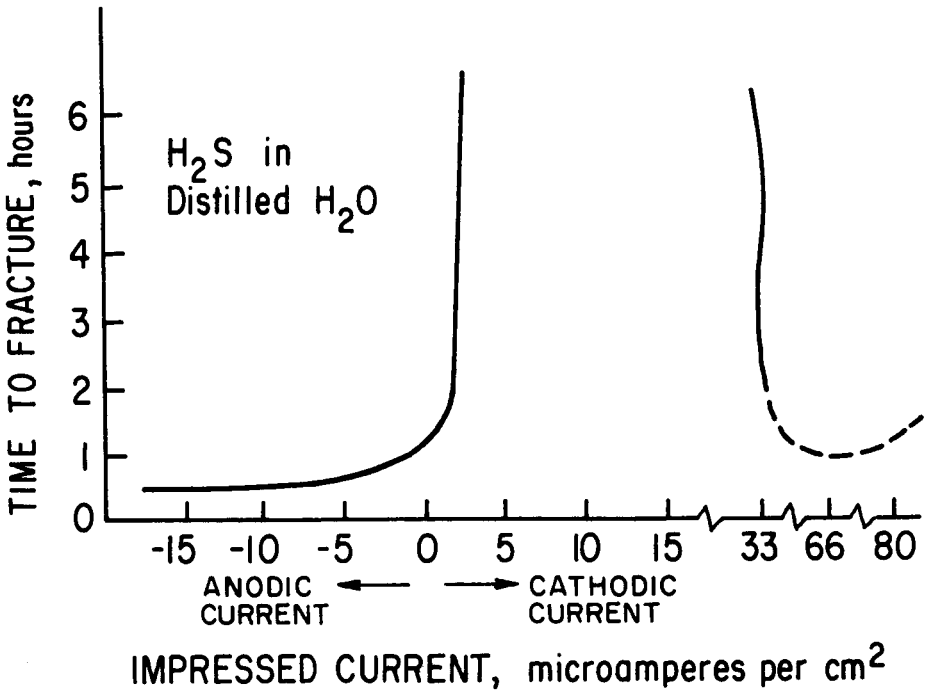
TIME TO FRACTURE, hours
0
1
2
3
4
5
6
H_2S in
Distilled H_2O
-15 -10 -5 0 5 10 15 33 66 80
ANODIC CURRENT
CATHODIC CURRENT
IMPRESSED CURRENT, microamperes per cm^2

(b)

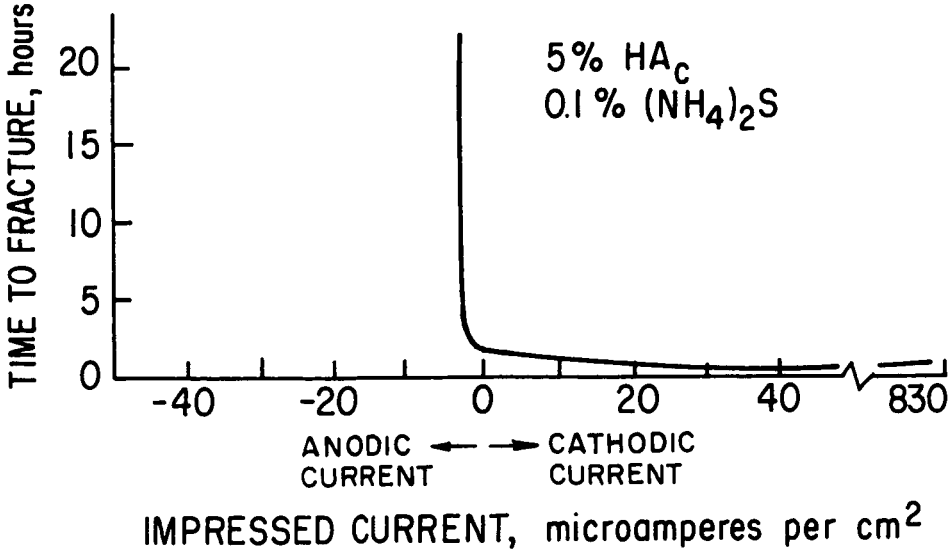
TIME TO FRACTURE, hours
0
5
10
15
20
5% HA_c
0.1 % $(NH_4)_2S$
-40 -20 0 20 40 830
ANODIC CURRENT
CATHODIC CURRENT
IMPRESSED CURRENT, microamperes per cm^2

FIGURE 16

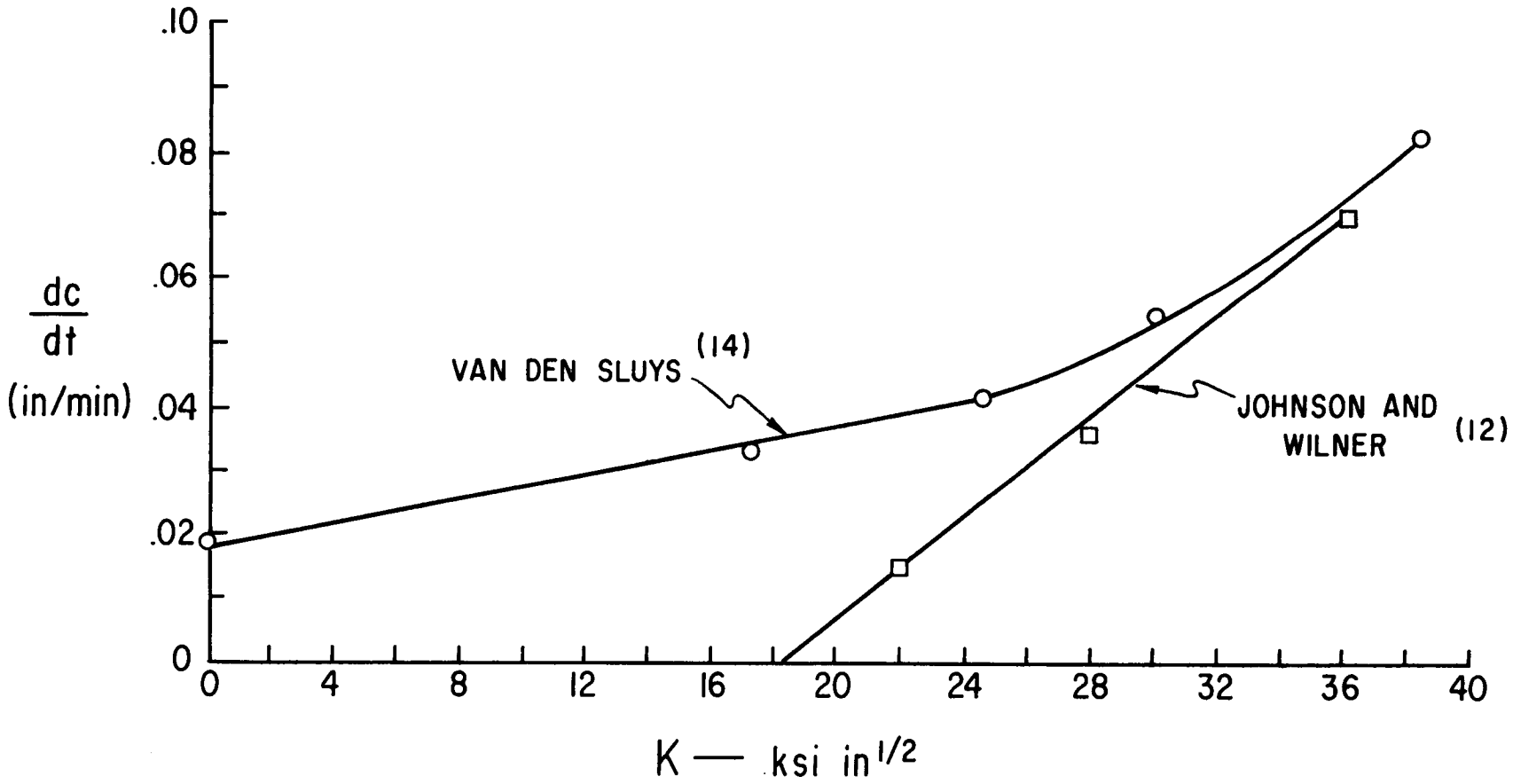
.10
.08
.06
.04
.02
0
dc/dt (in/min)
VAN DEN SLUYS (14)
JOHNSON AND WILNER (12)
0
4
8
12
16
20
24
28
32
36
40
K — ksi in^1/2

FIGURE 17

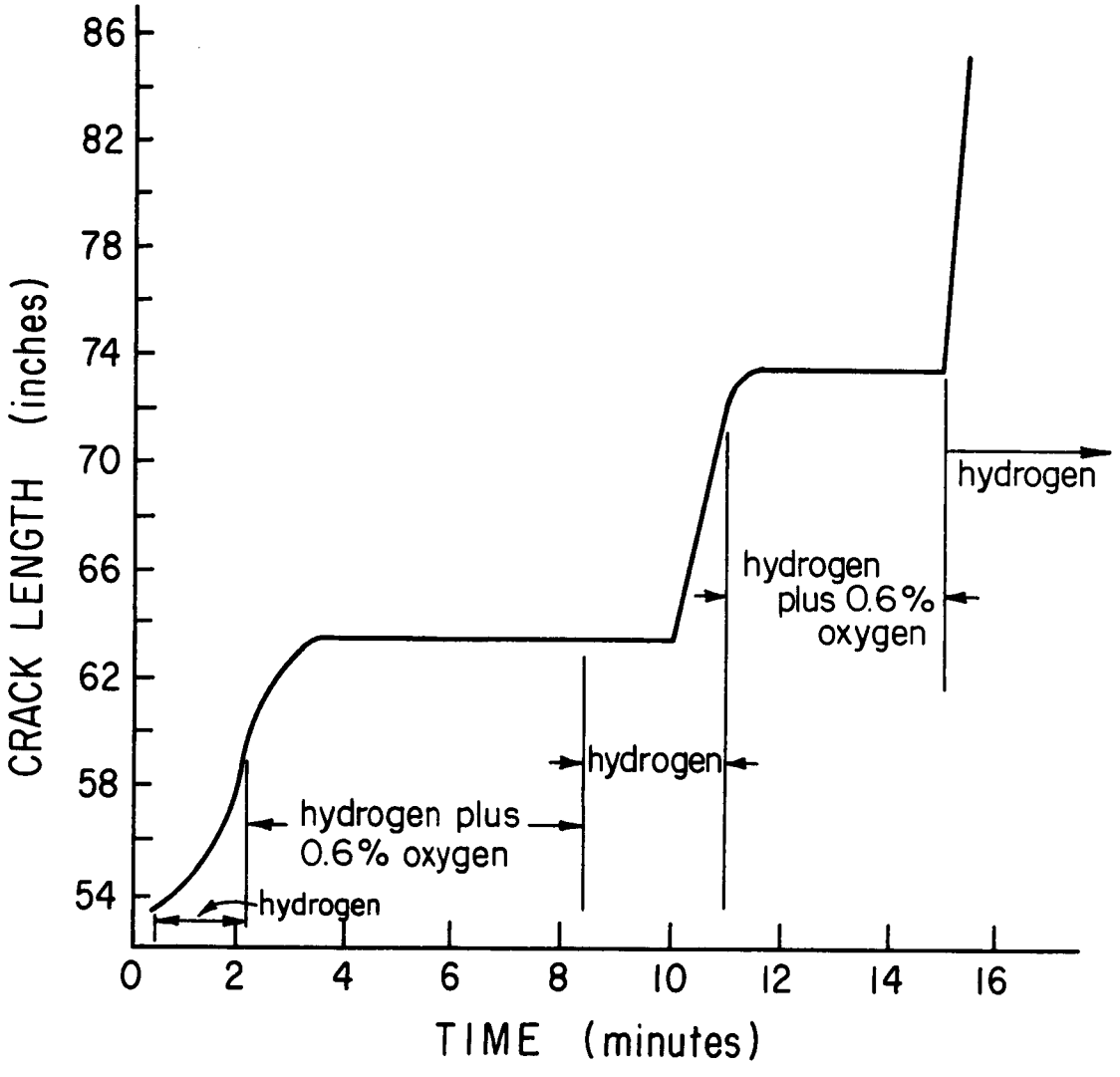
86
82
78
74
70
66
62
58
54
CRACK LENGTH (inches)
0
2
4
6
8
10
12
14
16
TIME (minutes)
hydrogen
hydrogen plus
0.6% oxygen
hydrogen
hydrogen
plus 0.6%
oxygen
hydrogen

FIGURE 18